Article

Current Biology

Auditory Corticothalamic Neurons Are Recruited by Motor Preparatory Inputs

Graphical Abstract

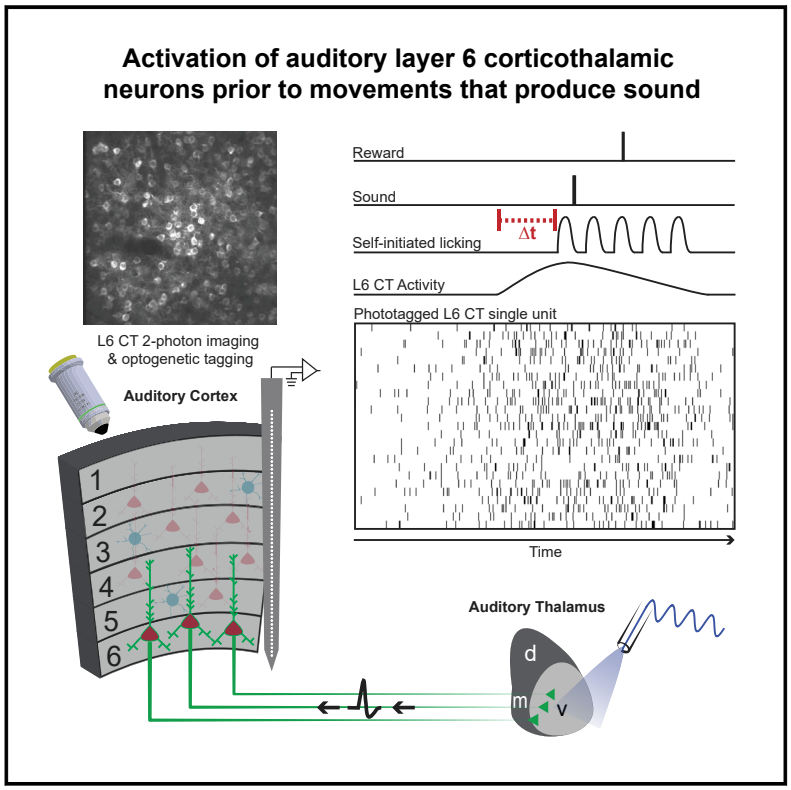

Highlights

- L6 corticothalamic neurons (L6 CTs) were isolated during active listening tasks
- L6 CT activity increases prior to movements that trigger sound and reward
- Motor corollary input activates L6 CTs at similar latency to FS interneurons
- Rabies tracing reveals monosynaptic inputs onto L6 CTs from globus pallidus

Authors

Kameron K. Clayton, Ross S. Williamson, Kenneth E. Hancock, Gen-ichi Tasaka, Adi Mizrahi, Troy A. Hackett, Daniel B. Polley

Correspondence

daniel_polley@meei.harvard.edu

In Brief

Corticothalamic neurons (CTs) regulate excitability throughout the thalamocortical loop, but what regulates *their* excitability? Clayton et al. record from mouse auditory layer 6 CTs during active listening tasks. They find strong motor-related extra-sensory activation of layer 6 CTs beginning hundreds of milliseconds prior to movement onset.

Clayton et al., 2021, Current Biology *31*, 1–13
January 25, 2021
https://doi.org/10.1016/j.cub.2020.10.027

CellPress

Please cite this article in press as: Clayton et al., Auditory Corticothalamic Neurons Are Recruited by Motor Preparatory Inputs, Current Biology (2020), https://doi.org/10.1016/j.cub.2020.10.027

Current Biology

CellPress

Article

Auditory Corticothalamic Neurons Are Recruited by Motor Preparatory Inputs

Kameron K. Clayton,[1] Ross S. Williamson,[1,2,5] Kenneth E. Hancock,[1,2] Gen-ichi Tasaka,[3] Adi Mizrahi,[3] Troy A. Hackett,[4] and Daniel B. Polley[1,2,6,*]

[1]Eaton-Peabody Laboratories, Massachusetts Eye and Ear Infirmary, Boston, MA 02114, USA
[2]Department of Otolaryngology – Head and Neck Surgery, Harvard Medical School, Boston, MA 02114, USA
[3]Department of Neurobiology, The Edmond and Lily Safra Center for Brain Sciences, The Hebrew University of Jerusalem, Jerusalem 91904, Israel
[4]Department of Hearing and Speech Sciences, Vanderbilt University Medical Center, Nashville, TN 37203, USA
[5]Present address: Department of Otolaryngology, University of Pittsburgh, Pittsburgh, PA, USA
[6]Lead Contact
*Correspondence: daniel_polley@meei.harvard.edu
https://doi.org/10.1016/j.cub.2020.10.027

SUMMARY

Corticothalamic (CT) neurons comprise the largest component of the descending sensory corticofugal pathway, but their contributions to brain function and behavior remain an unsolved mystery. To address the hypothesis that layer 6 (L6) CTs may be activated by extra-sensory inputs prior to anticipated sounds, we performed optogenetically targeted single-unit recordings and two-photon imaging of Ntsr1-Cre+ L6 CT neurons in the primary auditory cortex (A1) while mice were engaged in an active listening task. We found that L6 CTs and other L6 units began spiking hundreds of milliseconds prior to orofacial movements linked to sound presentation and reward, but not to other movements such as locomotion, which were not linked to an explicit behavioral task. Rabies tracing of monosynaptic inputs to A1 L6 CT neurons revealed a narrow strip of cholinergic and non-cholinergic projection neurons in the external globus pallidus, suggesting a potential source of motor-related input. These findings identify new pathways and local circuits for motor modulation of sound processing and suggest a new role for CT neurons in active sensing.

INTRODUCTION

Beginning with the early descriptions of Ramon y Cajal, anatomists have noted the massive network of descending corticofugal neurons in the deep layers of sensory cortex that innervate the thalamus, midbrain, and brainstem.[1] A set of organizing principles that describe sensory corticofugal contributions to perception and adaptive behaviors has remained elusive due to the technical challenges of monitoring or selectively manipulating targeted cell types in the deepest layers of the cortex in behaving animals. The advent of optogenetic approaches to activate and silence layer 6 corticothalamic (L6 CT) neurons in Ntsr1-Cre transgenic mice reinvigorated research on corticofugal circuits, inspiring new hypotheses about their role in sensory gain control and predictive coding.[2–7] Optogenetic stimulation or inactivation of Ntsr1-Cre+ neurons has demonstrated that L6 CTs are not subtle modulators of downstream activity, but instead throttle the excitability of thalamic and cortical circuits through their direct connections onto combinations of excitatory and inhibitory cell types in each brain region.[2–4,8–13]

Conventional optogenetic stimulation induces artificial patterns of spatiotemporal activity that do not resemble natural spiking, but these experiments can identify testable hypotheses about the type of firing patterns that might be naturally employed during particular behavioral states. A key concept to emerge from studies of L6 CT neurons is that they can exert either net excitatory or net suppressive effects on downstream circuits, depending on the timing of activation.[3,4,11] For example, our prior work found that activation of L6 CTs in the auditory cortex (ACtx) could either suppress or enhance sound-evoked activity in the thalamus and cortex and bi-directionally modulate perceptual thresholds for sound detection and discrimination.[4] The strongest effects on neural responses and perception occurred *after* optogenetically induced L6 CT spiking ended, not during activation, and the specific form of modulation (i.e., suppression or enhancement) depended on the temporal interval between the offset of L6 CT spiking and the arrival of auditory stimulation.

Because the largest and clearest effects of L6 CT activation on auditory thalamocortical tuning and perception occurred after their photoactivated spike volleys ended, we speculated that L6 CT neurons might be naturally recruited to spike prior to anticipated sounds during active sensing. Here, we report that L6 CTs in the mouse primary auditory cortex (A1) can resemble motor cortex neurons, in the sense that their activity often ramped up hundreds of milliseconds prior to the onset of movements linked to sound generation. The timing of L6 CT activation was temporally aligned with motor-related recruitment of fast-spiking (FS) interneurons, which was reported in previous work to reflect motor corollary discharge from the secondary motor cortex (M2).[14] Using rabies-based monosynaptic input tracing, we identified numerous inputs from the globus pallidus onto A1 L6 CT cells, but only sparse inputs from M2. These findings suggest new

Please cite this article in press as: Clayton et al., Auditory Corticothalamic Neurons Are Recruited by Motor Preparatory Inputs, Current Biology (2020), https://doi.org/10.1016/j.cub.2020.10.027

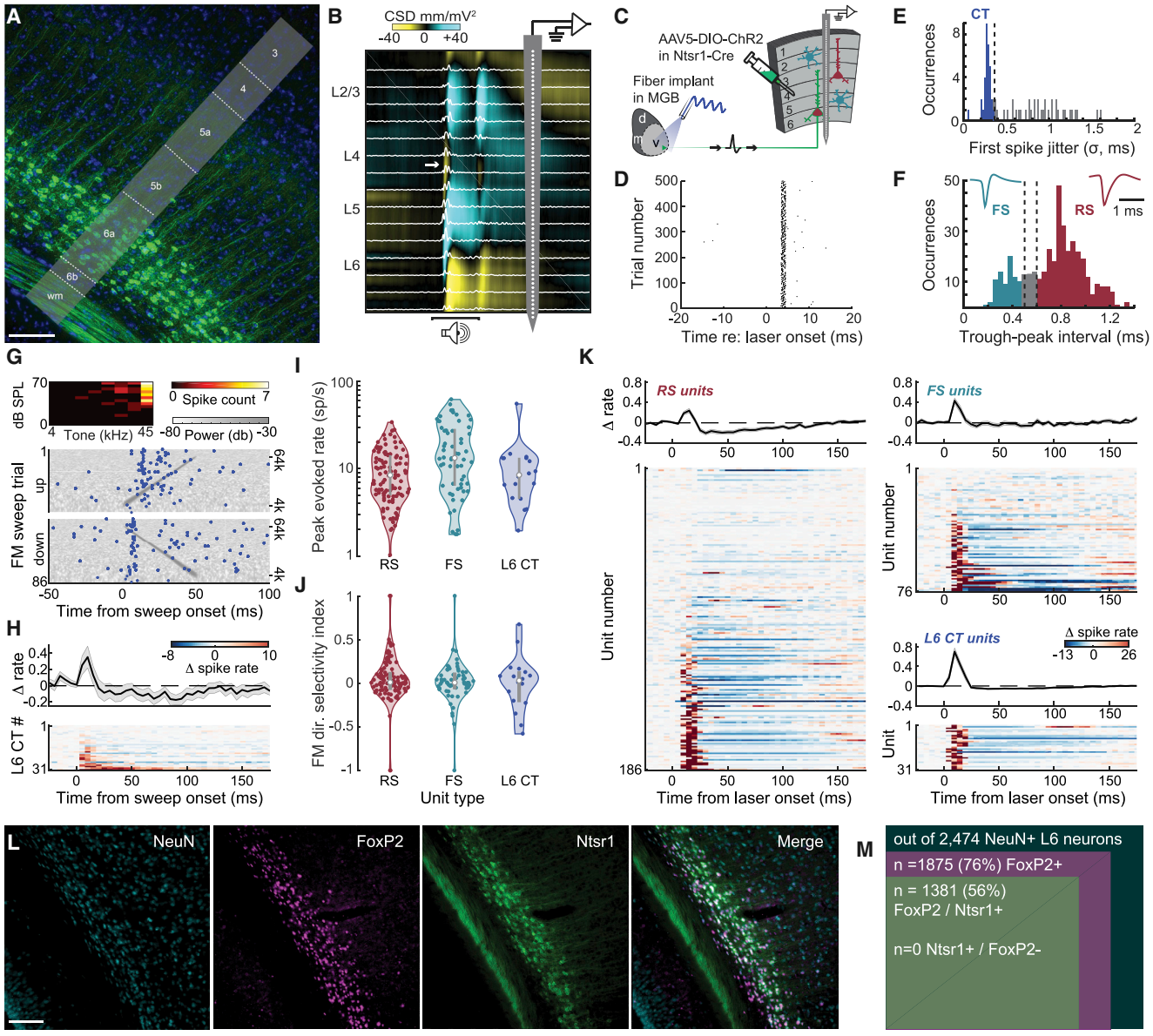

Figure 1. Histological and Functional Characterization of A1 L6 CT Neurons

(A) A1 corticothalamic cells labeled in NTSR1-Cre x Ai148 mice have somata in L6a and sparse vertically oriented neuropil labeling up to L5a. Scale bar, 0.1 mm.

(B) Extracellular recordings were made from all layers of A1 with a 64-channel linear probe. Electrophysiological responses are filtered offline to separately analyze unit spiking (white trace) and the current source density (CSD). White arrow in CSD trace identifies the early current sink in layer L4 elicited by a 50-ms white noise burst used to assign units to layers.

(C) Schematic for antidromic optogenetic phototagging in NTSR1-Cre+ L6 corticothalamic neurons that express ChR2.

(D) Rastergram of antidromic spikes elicited by photoactivation of thalamic axon terminals of an example L6 corticothalamic unit.

(E) Histogram of first-spike latency jitter in 77 units with optogenetically evoked responses. Directly activated L6 corticothalamic cells were distinguished from indirectly activated units as having a jitter in first-spike latency less than 0.35 ms (dashed vertical line).

(F) Isolated single units were classified as FS or RS (trough-to-peak delay < 0.5 ms or > 0.6 ms, dashed vertical lines). Spike waveforms reflect mean FS and RS waveforms.

(G) Sensory tuning from an example L6 CT unit. Top: brief tone pips identified a high-frequency receptive field. Bottom: FM sweep-evoked spiking rastergrams are superimposed on spectrograms of upward and downward FM sweeps in continuous white noise.

(H) Mean ± SEM normalized firing rates (top) and individual unit firing rates (bottom) relative to a pre-stimulus baseline for all phototagged L6 CT units (n = 31).

(I) Peak firing rates elicited by the average of up and down FM sweeps in 108 RS, 60 FS, and 18 significantly responsive L6 CT single units. Firing rates varied significantly between cell types (one-way ANOVA, $F = 7.83$, $p = 0.0005$). Post hoc pairwise comparisons confirmed similar firing rates in L6 CT and other RS units ($p = 1$). Normalized histogram violin plots present the median value as the white circle and the interquartile range as the gray vertical bars.

(J) FM direction selectivity index ([up − down] / [up + down]) is similar across sound-responsive cell types (one-way ANOVA, $F = 0.6$, $p = 0.55$).

(legend continued on next page)

Please cite this article in press as: Clayton et al., Auditory Corticothalamic Neurons Are Recruited by Motor Preparatory Inputs, Current Biology (2020), https://doi.org/10.1016/j.cub.2020.10.027

pathways and local circuits for modulating cortical sound processing during active sensing behaviors.

RESULTS

In the ACtx, L6 CT axons bifurcate into a subcortical branch that deposits collaterals onto GABAergic neurons in the thalamic reticular nucleus en route to the medial geniculate body (MGB) and a slender, vertically oriented intracortical branch that predominantly collateralizes within layers 5a and 6 of the local column (Figure 1A).[4,15–18] Here, we used an optogenetic approach to antidromically identify or "phototag" L6 CT neurons in A1 of awake, head-fixed mice by recording from all layers of the cortical column with high-density 64-channel linear probes (Figure 1B).[12,19–21] Several weeks prior, we expressed channelrhodopsin-2 in Ntsr1-Cre+ L6 CT neurons and implanted an optic fiber such that the tip terminated above the dorsal surface of the MGB (Figure 1C). This allowed us to optogenetically activate the thalamic axon terminals of L6 CT neurons with a brief (1 ms) flash of blue light and quantify the temporal jitter of antidromic spikes recorded from A1 cell bodies (Figure 1D). As confirmed in our recent study, units with minimal trial-to-trial jitter in first-spike latency were operationally defined as Ntsr1-Cre+ L6 CT units directly activated by the laser pulse (Figure 1E).[12] Units that did not respond to the laser or responded with higher first-spike jitter (>0.35 ms) were classified by their spike waveform shape as regular spiking (RS) or putative parvalbumin-expressing GABAergic FS neurons (Figure 1F). Of the 32 optogenetically identified L6 CT units, all were recorded on contacts in L6 based on the current source density (CSD) pattern (Figure 1B), and none had a trough-to-peak interval in the range of FS neurons (<0.5 ms), supporting our ability to isolate the action potentials of L6 CTs based on extracellular recordings.

As a first step, we measured sensory response properties of L6 CT neurons in comparison to other FS and RS units in the same vertical column while mice were alert, but not moving. We probed the sensory tuning properties using a combination of pure tones and frequency-modulated (FM) sweeps in a background of continuous white noise (Figure 1G). A subset of optogenetically tagged L6 CT units (n = 18/32 significantly responsive/recorded) exhibited brisk, short-latency responses to FM sweeps (Figure 1H). FM-evoked responses in L6 CTs were not significantly different than other RS units (n = 108/259) or FS units (n = 60/93), either in terms of evoked firing rates (Figure 1I) or FM direction selectivity (Figure 1J, statistical reporting provided in figure legends). These observations confirm prior work in the auditory[12] and visual[22] cortex, by showing that—when it comes to sensory tuning—Ntsr1-Cre+ neurons are not categorically different than other RS pyramidal neurons found in other cortical layers.

The clearest distinguishing feature of L6 CTs was not their sensory response profiles, but rather that photoactivating their axons with just a 1-ms pulse of blue light was sufficient to produce an initial wave of intense excitatory responses followed by a prolonged period of suppression in RS and FS units within the vertical column (Figure 1K). As reported previously, sustained periods of local response modulation after laser offset are not observed with photoactivation of other types of corticofugal projection neurons, interneurons, or neuromodulatory inputs.[4,12,23]

We were intrigued by the idea that non-auditory inputs could naturally play the role of our laser pulse by recruiting L6 CT neurons to spike shortly before the onset of upcoming acoustic events. We were particularly struck by the nearly perfect co-expression of the forkhead box protein P2 (FoxP2) in cortical Ntsr1-Cre+ neurons,[24,25] a protein that—in mice—is highly enriched in motor control nuclei and distributed brain regions that integrate sensory inputs with motor-related signals.[26] The selective expression of FoxP2 in Ntsr1-Cre neurons reported in other cortical areas led us to question whether the activity of L6 CT neurons might be best understood in the context of sensorimotor integration. As a first step, we immunolabeled A1 sections from Ntsr1-Cre × Ai148 mice and confirmed that FoxP2 was also highly expressed in A1, but only in L6 (Figure 1L). Further, we found that 74% of L6 FoxP2 neurons in A1 (1381/1875) were Ntsr1-Cre+ and—strikingly—every Ntsr1-Cre+ neuron expressed FoxP2 (Figure 1M). The strong co-expression of FoxP2 in Ntsr1-Cre+ neurons motivated us to ask whether movement—or internal motor corollary inputs that precede movement—could be a naturally occurring source of extra-sensory input for L6 CTs that would cause them to fire in advance of auditory stimuli.

Characterizing a Highly Stereotyped, Self-Initiated, Rapid-Onset Movement

To characterize the degree and timing of L6 CT activation in an audiomotor task, we sought to have mice spontaneously, rapidly, and repeatedly deploy a highly stereotyped movement to trigger a brief sound. To this end, we used a minimalistic lick spout sampling task in which tongue contact on a lick spout had a 50% probability of generating an FM sweep and a 50% probability of resulting in a water reward (each independently determined). Sound onset was delayed by 0.1 s following lick bout initiation on trials that combined sound and movement. Water reward was delivered 0.5 s after lick spout contact on the fraction of trials that culminated in reinforcement. Continuous background masking noise obscured sound arising from the lick itself. This task design motivated mice to perform many trials per day, while allowing us to separate trials with various permutations of lick events, sound stimuli, and reinforcement. Although our primary motivation was to study the influence of movement on A1 activity, we confirmed that sound-evoked A1 responses were suppressed during licking when compared with the responses to sounds presented while the mouse was still, consistent with many prior reports of suppressed sound-evoked activity during whole body movements including locomotion and bar pressing (Figure S1).[14,27–31]

(K) Neurograms, grouped by cell type, present the firing rate change relative to baseline before and after photoactivation of L6 CT units with a 1-ms pulse of light. Units are sorted by the absolute value of their mean activity. Line plots present the mean ± SEM normalized firing rates relative to a pre-stimulus baseline for RS, FS, and L6 CT cell types.

(L) A1 cells in NTSR1-Cre x Ai148 mice were immunolabeled for NeuN and FoxP2. Scale bar, 0.1 mm.

(M) Venn diagram depicts the co-localization of FoxP2 in A1 L6 neurons and NTSR1-Cre in FoxP2+ and FoxP2− L6 neurons.

Please cite this article in press as: Clayton et al., Auditory Corticothalamic Neurons Are Recruited by Motor Preparatory Inputs, Current Biology (2020), https://doi.org/10.1016/j.cub.2020.10.027

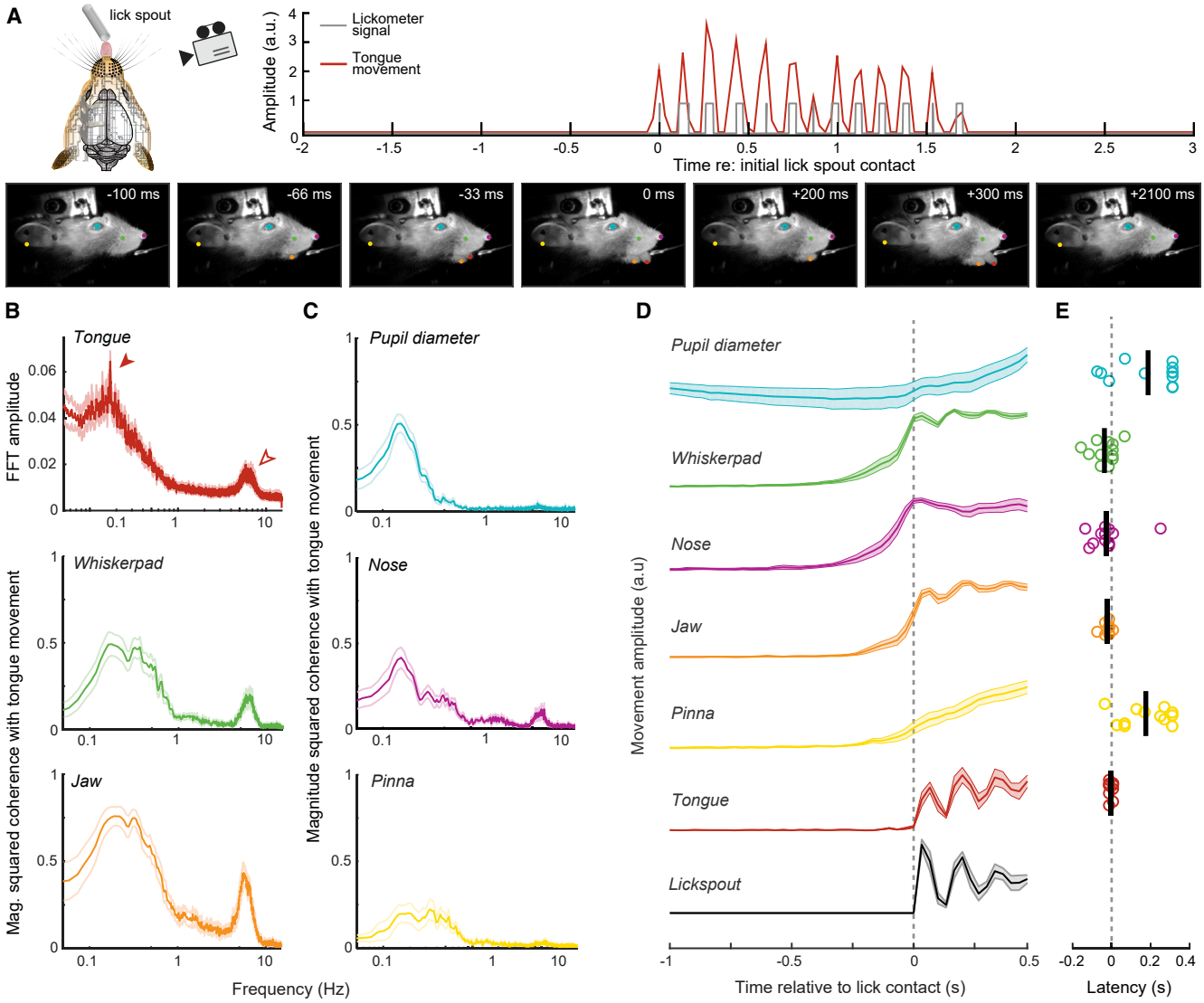

Figure 2. Quantification of a Stereotyped, Self-Initiated, Rapid-Onset Movement Sequence Culminating in Lickspout Contact

(A) Quantitative videography of facial movements surrounding lick spout contacts was performed with DeepLabCut. Top right: data from a representative trial indicates that tongue movement from video analysis (maroon) is plotted relative to electrical contacts of the tongue contact on the lick spout (gray). Bottom: DeepLabCut marker positions are indicated for the pinna, whisker pad, nose, tongue, jaw, and pupil in seven individual video frames.

(B) Mean ± SEM amplitude spectrum for the tongue movement signal taken from the duration of each session across all mice (n = 12 video sessions from 4 mice). Closed and open arrowheads denote the frequency of overall lick bouts and individual licks, respectively.

(C) Mean ± SEM magnitude-squared coherence between tongue movement and pupil diameter and other facial markers across the duration of each behavioral measurement session.

(D) Mean ± SEM movement amplitudes and pupil diameter are shown relative to electrical contact with the lickspout (dashed gray line).

(E) Onset latencies for initial changes in facial markers and pupil diameter relative to lickspout contact. Each data point represents a single imaging session. Black vertical bar = sample mean. Dashed gray line = time of electrical contact with lick spout.

To quantify the timing of orofacial movements and pupil diameter preceding lick bout onset, we used DeepLabCut, a video analysis method for markerless tracking of body movements based on deep neural networks (n = 12; three videography sessions in each of four mice).[32,33] We found that licks were deployed in bouts, each 1–2 s in duration, composed of multiple individual licks (Figure 2A). A Fourier analysis of the tongue movement identified two peaks at approximately 0.1 and 7 Hz, which correspond to the lick bouts and individual licks, respectively (Figure 2B). Focusing only on trials where water rewards were omitted, we observed a reproducible sequence of orofacial movements associated with lick bout initiation. Whereas movement of the whisker pad, nose, and jaw reliably tracked both the overall bouts and individual licks, pupil diameter changes corresponded only to the overall lick bout, and pinna movements were generally less coherent with licking (Figure 2C). Analyzing the movement over time relative to lick bout onset, we found that the whisker pad, nose, and lower jaw reliably

Please cite this article in press as: Clayton et al., Auditory Corticothalamic Neurons Are Recruited by Motor Preparatory Inputs, Current Biology (2020), https://doi.org/10.1016/j.cub.2020.10.027

preceded lick spout contact, whereas changes in pupil diameter and pinna movement lagged behind lick bout onset (Figure 2D). Based on this evidence, we proceeded with recording from A1 single units during the lick spout sampling task, knowing that the earliest overt facial movements preceded lick spout contact by approximately 30 ms (Figure 2E).

Motor Preparatory Inputs Activate Deep-Layer A1 Neurons

Suppression of sound-evoked activity in ACtx RS units during movement is thought to arise, in part, from increased spiking of FS and other local inhibitory neurons prior to movement onset.[14] Given the persistent suppressive effect of L6 CT photoactivation on RS units (Figure 1K), we reasoned that L6 CT units may also be recruited to fire prior to movement onset. As a next step, we characterized the degree and timing of firing rate changes in L6 CT, RS, and FS units prior to the onset of self-initiated lick bouts. We found that significantly suppressed spiking during licking was observed in roughly 25% of units and was expressed similarly across layers (n = 28, 43, 132, and 135 units in L23, L4, L5, and L6, respectively; Figure 3A). Firing rates were significantly increased in approximately 40% of single units, particularly in L6, where spiking ramped up hundreds of milliseconds before contact with the lick spout. Firing rate changes in FS units increased prior to movement, but were not different across layers (n = 79, mixed design ANOVA, main effect for time and layer, $F = 4.03$ and 2.06, $p < 1 \times 10^{-6}$ and 0.11, respectively; time × layer interaction term, $F = 0.93$, $p = 0.65$). RS unit activity increased overall prior to lick onset (main effect for time, $F = 4.29$, $p < 1 \times 10^{-6}$), but this was mainly attributable to strong motor-related activation of L6 RS units (n = 236, main effect for layer, $F = 2.66$, $p = 0.04$; time × layer interaction term, $F = 1.58$, $p < 0.001$). Focusing only on L5 and L6, we confirmed prior reports that FS firing rates increased over a 1-s period prior to movement onset without any systematic differences across layers (Figure 3B).[14,29,30] We observed that a minority of RS units were suppressed shortly prior to lick onset, but the most salient observation was the sub-population of L6 RS units that increased their spiking at approximately the same time as FS units (Figure 3B, bottom).

To determine the onset latency of motor-related spiking, we followed the analysis approach of prior reports and replicated the finding that FS units activated by movement first begin to increase their spiking hundreds of milliseconds prior to movement onset (mean latency for L2/3, L5, L6 FS units = −292 ms, −400 ms, −396 ms; Figure 3C).[14] Motor-related changes in RS unit spiking lagged behind FS units with one notable exception: L6 RS units began to increase their spiking at approximately the same latency as FS units (−349 ms prior to lick spout contact; unpaired t test for enhanced L6 RS versus FS latencies, $p = 0.63$). As the earliest changes in FS and L6 RS firing rates begin more than an order of magnitude earlier than the beginning of orofacial movements, they reflect motor-preparatory-related activity rather than sensory feedback arising from ongoing movements. Firing rate changes after licking offset largely mirrored onset effects; spiking persisted for hundreds of milliseconds after the final lick spout contact in L6 and, to a lesser extent, in L5, but not in L2/3 or L4 (Figure S2).

To determine if motor-preparatory recruitment of L6 RS units included L6 CTs, we separately analyzed motor-related activity changes in optogenetically phototagged neurons (n = 32, N = 6 mice; Figure 3D). Latencies for motor-related enhancement or suppression were not significantly different than unidentified L6 RS units, which is unsurprising given that the majority of L6 RS units are CT neurons (Figure 3E). These results demonstrate that L6 Ntsr1-Cre+ CTs (and possibly other sub-types of deep-layer RS units) begin to ramp up their spiking in response to motor corollary inputs hundreds of milliseconds prior to movement onset.

Motor-Preparatory Inputs Activate L6 CT Ensembles

Single-unit recordings measure spiking at millisecond resolution, which is useful when calculating onset latencies for neural changes relative to overt movements. However, the yield in single-unit recording experiments is much lower than two-photon imaging, particularly with antidromic phototagging, where we optogenetically tagged less than one CT unit on average in any given recording session. Although the comparatively sluggish time constants and uncertain spike coupling with calcium indicators preclude any strong claims about the precise timing of neural activity and movement, we extended our motor characterization experiments with two-photon imaging to simultaneously visualize larger neural ensembles (Figure 4A).

Consistent with our small sample of L2/3 single-unit recordings (Figures 3B and 3C), orofacial movements elicited weak responses in L2/3 excitatory pyramidal neurons, with 68% of cells not significantly affected by movement, and the remainder of cells mostly activated or suppressed after the lick bout had begun (n = 624, N = 5; Figure 4B). Two-photon imaging of L6 cell bodies is impossible under most circumstances on account of fluorescence from superficial layers that greatly reduces the signal-to-noise ratio of somatic GCaMP signals. Because GCaMP expression is limited to upper L6 in Ntsr1-Cre × Ai148 mice and because these CT cells have sparse, slender, and short apical dendritic and axonal fields (Figure 1A), there is very little out-of-plane fluorescence, permitting two-photon calcium imaging at depths of ~0.7 mm without using high excitation laser power (Figure 4C).[5,22,34,35] In agreement with our phototagged recordings, we found that L6 CT neurons were strongly recruited by orofacial movements, where the activity rates of 74% of cells was significantly changed from baseline, mostly reflecting enhanced activity beginning prior to lick spout contact (n = 739, N = 3; Figure 4D).

Motor-Related Activation of L6 CTs Is Not Observed during Locomotion

We next addressed whether L6 CTs would be recruited by motor preparatory signals in a completely different motor behavior involving neither orofacial movements, nor a generalized expectation of reward. Self-initiated running on treadmills has been widely used to demonstrate motor-related activation in subcortical auditory stations[36] and recruitment of local ACtx circuits.[14,28,30,31,37] Like the lick spout sampling task, the onset of running (operationally defined as exceeding 2cm/s) triggered an FM sweep in 50% of trials. To avoid lick-related activity during running, the lick spout was removed from the test apparatus and water rewards were not provided. Two-photon imaging of Ntsr1-Cre+ neural ensemble neurons during the period leading up to self-initiated running bouts revealed virtually no motor-related recruitment of L6 CTs. Whereas 53% of L6 CT neurons showed

Please cite this article in press as: Clayton et al., Auditory Corticothalamic Neurons Are Recruited by Motor Preparatory Inputs, Current Biology (2020), https://doi.org/10.1016/j.cub.2020.10.027

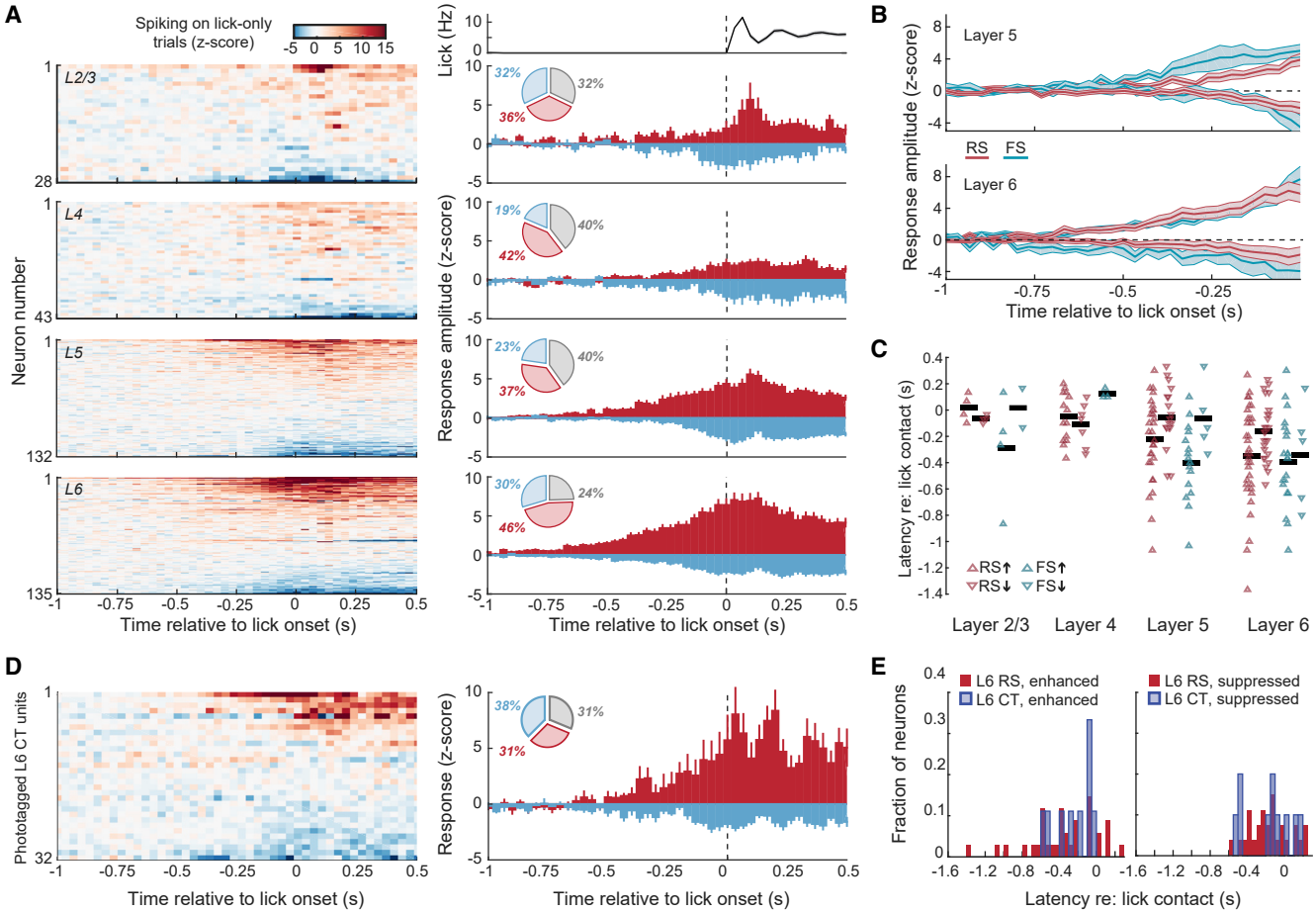

Figure 3. Motor-Preparatory Inputs Activate L6 Neurons in A1

(A) Left: neurograms are grouped by layer and present normalized spike rates for all single units on lick-only trials. Units are sorted by mean normalized activity. Right: pie charts present percentage of units significantly enhanced (red) or suppressed (blue) during the peri-lick period. PSTHs present mean ± SEM normalized firing rates for enhanced and suppressed units from the corresponding layer. Top panel presents the mean ± SEM lick rate during the recording sessions. Firing rate changes among significantly suppressed units were not different across layers (n = 28 L2/3, 43 L4,132 L5, and 135 L6 units; ANOVA, main effect for layer $F = 1.19$, $p = 0.7$). Firing rate changes among enhanced units differed between layers and was greatest in L6 (ANOVA, main effect for layer, $F = 8.55$, $p < 0.00003$; post hoc pairwise comparisons with Holm-Bonferroni correction, $p = 0.02$, 0.00009 and 0.02 for L6 versus L5, L4, and L2/3, respectively). Sound-evoked responses elicited during licking are suppressed relative to responses while at rest, but the suppression reflects a different laminar pattern (Figure S1). The decay of movement-related spiking relative to lick bout offset in lick-only trials is presented in Figure S2.

(B) Mean ± SEM changes in activity for all L5 (top) and L6 (bottom) RS and FS units that significantly increased or decreased their firing rates during lick-only trials.

(C) Motor-related response latencies for each significantly enhanced or suppressed single unit. Horizontal bar, sample mean.

(D) Motor-related recruitment of optogenetically identified L6 CT units. Neurogram, pie chart, and histogram plotting conventions match (A).

(E) Histograms of motor-related response latencies for all significantly enhanced (top) or suppressed (bottom) L6 CT units relative to other unidentified enhanced and suppressed RS L6 units. Motor-related firing rate latencies of enhanced and suppressed L6 CT units are not different than other unidentified enhanced and suppressed RS units (two-sample K-S tests on L6 CT versus L6 RS latency distributions, $p > 0.68$ for both enhanced and suppressed units).

significantly enhanced activity rates around the time of self-initiated lick bouts, only 15% showed significantly elevated activity around bouts of running (n = 606, N = 3; Figure 4E).

Put another way, L6 CTs showed similar patterns of motor-related activity to their L2/3 pyramidal neuron counterparts when the task emphasized bouts of running rather than orofacial movements (Figure 4F). However, the locomotion and lick spout sampling behaviors differ in many aspects other than movement type. For example, running-triggered sound delivery was less frequent than lick-triggered sound delivery (mean ± SEM movement-triggered FM sweeps per hour, 47.14 ± 5.1 versus 128.81 ± 16.41, for locomotion and lick spout sampling, respectively). Further to this point, mice were water deprived in the lick spout sampling task and had a generally increased expectation of water availability (145.23 ± 7.52 rewards per hour), whereas locomotion testing involved neither water restriction nor water delivery. These differences make it difficult to identify the precise feature that led to categorically different motor preparatory activation of L6 CT ensembles in these two behaviors, a point that we address further in Discussion.

Basal Ganglia Projections Target A1 L6 CT Neurons

As a final step, we investigated anatomical pathways that could potentially route motor-related inputs onto A1 L6 CT neurons.

Please cite this article in press as: Clayton et al., Auditory Corticothalamic Neurons Are Recruited by Motor Preparatory Inputs, Current Biology (2020), https://doi.org/10.1016/j.cub.2020.10.027

CellPress

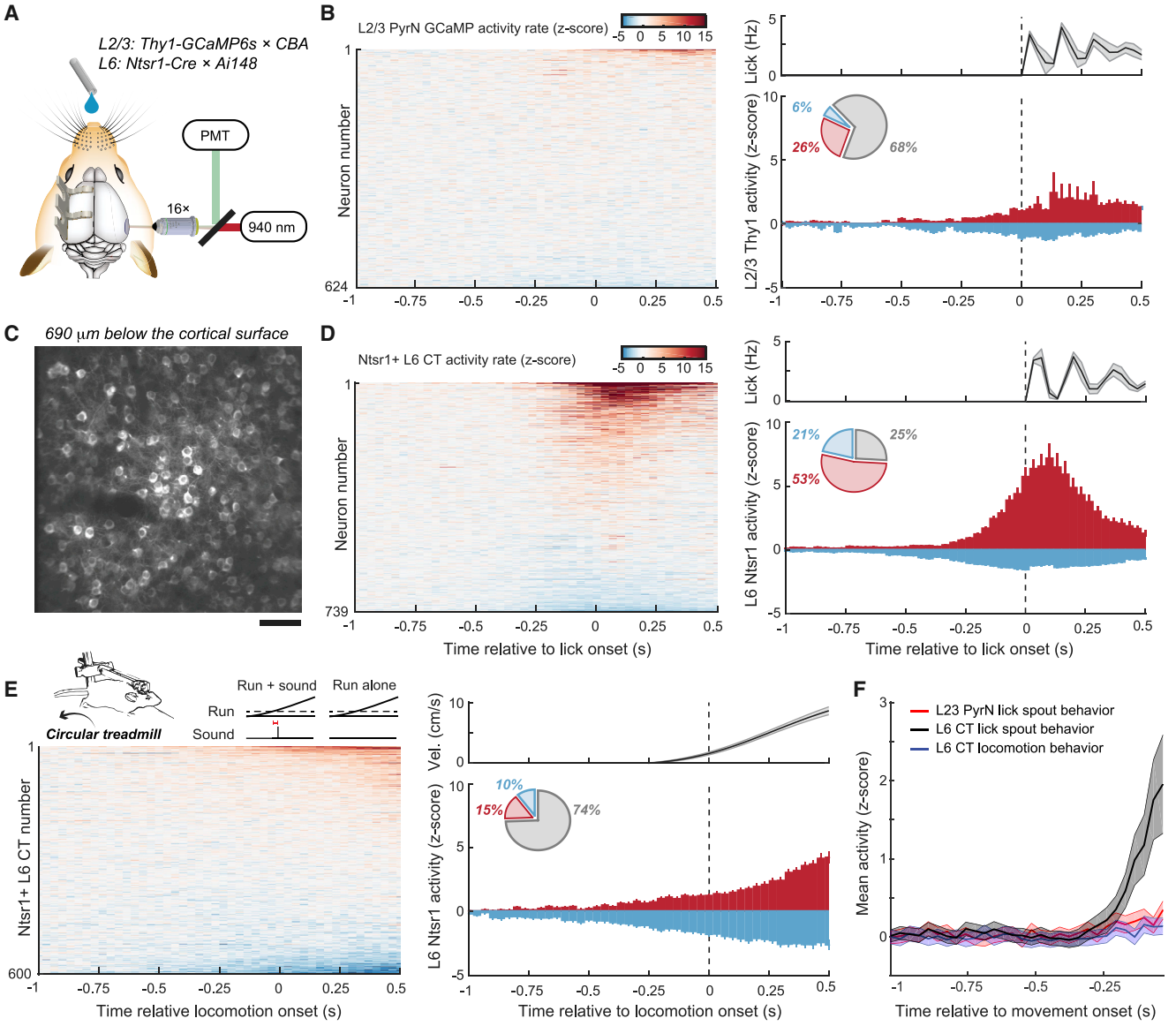

Figure 4. Ensembles of L6 CT Neurons Are Activated by Upcoming Orofacial Movements, but Not Locomotion Bouts

(A) Schematic for two-photon imaging of motor-related activation in L2/3 PyrNs and L6 corticothalamic neurons.

(B) Lick-related calcium activity from deconvolved GCaMP6 signals in L2/3 PyrNs. Left: neurograms present normalized activity rates for all L2/3 PyrNs on lick-only trials. Neurons are sorted by mean normalized activity. Right: pie charts present percentage of units significantly enhanced (red) or suppressed (blue) during the peri-lick period. PSTHs present mean ± SEM normalized activity rates. Top panel presents the mean ± SEM lick rate for the corresponding recordings sessions.

(C) GCaMP6 fluorescence in L6 corticothalamic cells in a NTSR1-Cre × Ai148 mouse. Scale bar, 50 μm.

(D) Lick-related calcium activity in L6 corticothalamic neurons. Graphing conventions match (B).

(E) Locomotion-related calcium activity in L6 corticothalamic neurons. Graphing conventions match (B). Top panel presents the mean ± SEM treadmill velocity from the corresponding recordings sessions.

(F) Mean ± SEM motor-related changes in PyrN activity for all two-photon imaging experiments. Activity was increased prior to movement onset, but only in L6 CTs and only for movements related to licking, not locomotion (mixed design ANOVA, time × group interaction, $F = 15.49$, $p = 2 \times 10^{-144}$).

Cholinergic projections from the caudal substantia innominata (SIn) make monosynaptic connections onto ACtx inhibitory neurons to suppress modulate cortical sound processing during states of movement, auditory learning, or active listening, though these inputs tend to lag (rather than lead) movement initiation.[37–39] The best-defined pathway for transmitting movement-related inputs into ACtx comes from neurons in M2 that make monosynaptic connections onto local inhibitory neurons to suppress pyramidal neuron responses prior to the initiation of self-generated sounds.[14,30,40] In addition to their monosynaptic inputs onto local GABA cells, M2 afferents also innervate deep layers of ACtx and reliably elicit excitatory

Please cite this article in press as: Clayton et al., Auditory Corticothalamic Neurons Are Recruited by Motor Preparatory Inputs, Current Biology (2020), https://doi.org/10.1016/j.cub.2020.10.027

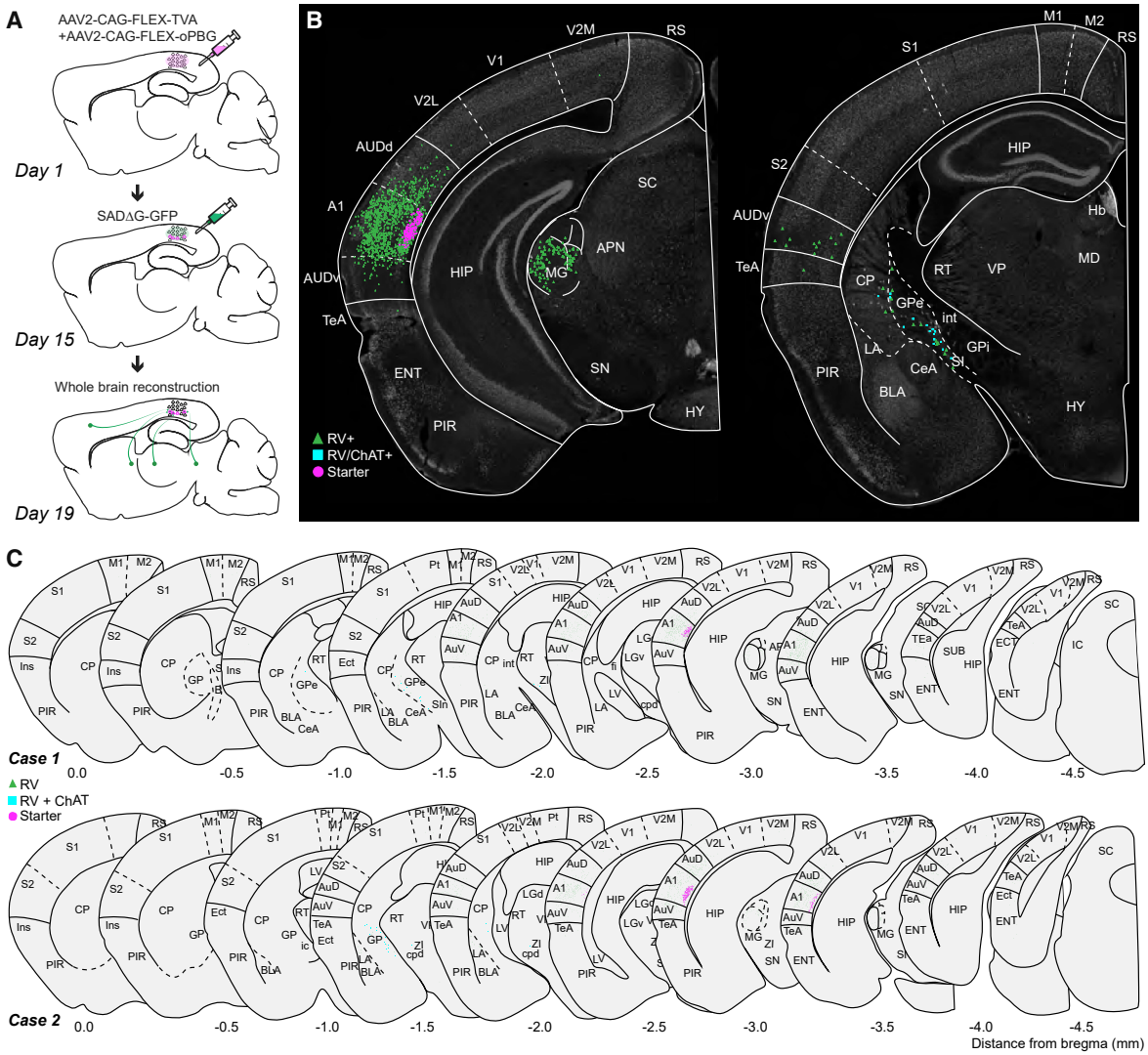

Figure 5. Brain-wide Sources of Monosynaptic Inputs onto A1 L6 Corticothalamic Neurons

(A) Schematic of viral labeling strategy to identify monosynaptic inputs onto Ntsr1-Cre L6 corticothalamic neurons.

(B) Two coronal sections showing L6 corticothalamic starter cells in A1 and RV-labeled monosynaptic inputs (RV+) in auditory forebrain (left) and a more rostral section containing the motor cortex and portions of the basal ganglia and basal forebrain (right).

(C) Coronal series from two mice showing reconstructions of all labeled cells.

(D) Proportion of RV-labeled input cells from the top-23 regions were independently calculated for each brain (N = 5). The number of L6 CT starter cells and RV+ input cells are provided in parentheses for each case in magenta and green, respectively. Gray bars = mean. Sensory cortical inputs: AUD = dorsal auditory area,

(legend continued on next page)

Please cite this article in press as: Clayton et al., Auditory Corticothalamic Neurons Are Recruited by Motor Preparatory Inputs, Current Biology (2020), https://doi.org/10.1016/j.cub.2020.10.027

synaptic currents in L6 pyramidal neurons,[40] though it has not yet been determined if these L6 cells are CTs and whether M2 input elicits net enhanced spiking rather than suppression in L6 RS neurons. A third possibility is the globus pallidus (GP), based on reports that GP firing rates are modulated before self-initiated movements.[41,42] The external GP borders the ACtx-projecting regions of SIn and contains a sub-compartment that projects to neocortex, including targeting of deep layer neurons in primary somatosensory cortex.[43,44] In rats, neurons in the external GP and caudate/putamen project to ACtx, though the cell-type-specific targets and the balance of projections to A1 versus other cortical fields have not yet been resolved.[45]

To identify long-range monosynaptic inputs onto A1 L6 CT neurons, we used RVdG-based *trans*-synaptic tracing.[46–48] Ntsr1-Cre+ L6 neurons were transduced with Cre-dependent viral constructs to become "starter cells" that express mCherry, the EnvA receptor TVA, and the rabies glycoprotein, G (AAV2-CAG-FLEx-TVA and AAV2-CAG-FLEx-oG, respectively; Figure 5A).[49,50] A second injection of an RVdG pseudotyped with an avian EnvA envelope protein (SADΔG-GFP) was made in the same A1 location to selectively transduce L6 CT starter neurons and drive GFP expression in their monosynaptic inputs. We confirmed that A1 L6 CTs are innervated by neighboring cortical regions, in addition to reciprocal inputs from ventral and medial divisions of the MGB, the same subdivisions targeted by their subcortical axons (Figure 5B, left).[18,51] As expected, we observed scattered inputs from SIn, but we also found input neurons in more central regions of GP, even as far dorsolateral as the caudate/putamen (Figure 5B, right). We quantified the brain-wide distribution of presynaptic inputs to A1 L6 CTs by sectioning at 40-μm resolution and reconstructing the location of all starter and input neurons (n = 1,628 starters and 22,625 input neurons in five mice; Figure 5C). As expected, the greatest number of inputs came from neighboring regions of ACtx, with a smaller fraction of inputs from a secondary visual field (Figure 5D).[52] In motor-related brain regions, approximately ten times more input cells were identified in GP than M2, suggesting an alternative pathway that could potentially route motor-related signals onto L6 CT neurons.

The majority of cells that project from the caudal tail of the basal forebrain and GP to various A1 cell types are cholinergic and are primarily localized to SIn, although there are a fringe of cholinergic cells extending dorsally and laterally that are not easily assigned to GP versus SIn (Figure 6A).[21,39,43,45,53] We quantified immunolabeled RV+/GFP+ input neurons and observed that approximately half of the GP and SIn inputs to A1 L6 CTs were non-cholinergic (Figure 6B). In the GP, non-cholinergic pallidocortical neurons are presumably GABAergic and receive both direct and indirect pathway input.[43] The functional contributions of these cholinergic and non-cholinergic projections to A1 L6 CTs in the context of motor-preparatory modulation or generalized internal state modulation awaits future targeted activation and inactivation experiments.

DISCUSSION

The use of modern neuroscience methods to interrogate Ntsr1-Cre+ neurons in the auditory, visual, and somatosensory cortex is beginning to reveal a new role for L6 CT neurons in sensory processing and perception. Our previous and current findings demonstrate that L6 CT neurons receive feedforward inputs from the first-order auditory thalamus, the ventral MGB (Figure 5D), have well-defined auditory tuning profiles[12] (Figures 1G–1J) and strongly express FoxP2, a protein marker found in brain regions involved in motor control and sensorimotor integration (Figures 1L and 1M). Ntsr1-Cre+ L6 CT neurons in the visual cortex also have well-defined visual receptive fields and express FoxP2.[22,24] Visually evoked responses in L6 CT neurons are strongly modulated by arousal state, as indexed by pupil diameter and locomotion, yet the onset of locomotion per se does not activate visual cortex L6 CT neurons,[22] as confirmed here in the auditory cortex (Figures 4E and 4F). Ntsr1-Cre+ neurons target a combination of inhibitory FS and putative excitatory RS pyramidal neurons, particularly in layers 5 and 6 of the local cortical column in auditory, visual, and somatosensory cortex.[4,8,9,12] Similarly, Ntsr1-Cre+ neurons strongly drive excitatory neurons in the first-order thalamic regions as well as inhibitory neurons in the thalamic reticular nucleus that then transmit delayed feedforward inhibition to the first-order thalamic regions.[3,4] Taken together, L6 CT neurons can both excite and suppress the activity of local circuits within the cortex (Figure 1K) and downstream circuits in the thalamus, where the net balance of the downstream effect may depend on how the L6 CT spikes are arranged in time or arranged relative to the timing of ascending sensory inputs.[3,4,11,13,54]

The principal question that motivated our work here was to identify inputs that naturally activate L6 CT neurons. Our previous work demonstrated that sound-evoked latencies in L6 CT units can lead other deep-layer corticofugal neuron types by approximately 7 ms,[12] but we were particularly motivated to understand whether there were types of inputs that could naturally elicit discrete bursts of L6 CT spiking that ended 50–150 ms prior to the arrival of auditory inputs, the time interval when optogenetic activation of L6 CT units has the strongest effects on thalamocortical stimulus processing and sound perception.[4] We interpreted the strong FoxP2 expression in Ntsr1-Cre+ neurons as a possible clue that motor-related input might activate L6 CTs and designed a lick spout sampling behavior in which tongue contact on the spout would occasionally trigger a sound 100 ms later. We confirmed our hypothesis that motor-related inputs elicit strong spiking responses in L6 CTs (as well as other L6 RS units), which may contribute to sound-evoked neural suppression elicited by sounds that follow lick spout contact (Figure S1). We also discovered that motor-related activity in L6 was distributed over time, and in that sense not like a discrete optogenetic input (Figures 3A and S2), but—more surprisingly—that the increase in activity

AUV = ventral auditory area, TEA = temporal association cortex, V1 = primary visual cortex, V2M/L = medial and lateral secondary visual area, and S1 and S2 = primary and secondary somatosensory cortex. Thalamic inputs: MGv/d/m = ventral, dorsal, and medial subdivisions of the medial geniculate body, Sg = suprageniuclate thalamic nucleus, PO = posterior thalamic nucleus, and ZI = zona incerta. Motor-related inputs: M1 and M2 = primary and secondary motor cortex, CP = caudate putamen, GP / GPe = external globus pallidus, and SIn = substantia innominata. Other: RS = retrosplenial cortex, ECT = ectorhinal cortex, ENT = entorhinal cortex, and LAdl = dorsolateral subdivision of the lateral amygdala.

Please cite this article in press as: Clayton et al., Auditory Corticothalamic Neurons Are Recruited by Motor Preparatory Inputs, Current Biology (2020), https://doi.org/10.1016/j.cub.2020.10.027

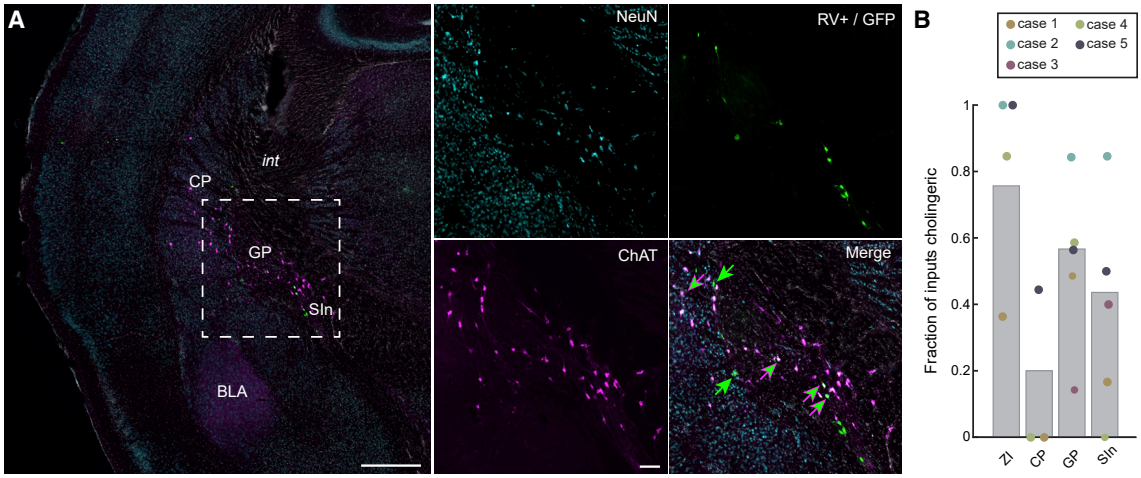

Figure 6. A Mixture of Cholinergic and Non-cholinergic Cells Project to A1 L6 Corticothalamic Neurons

(A) Higher magnification image showing the caudal tail of GP and SIn from an example brain. RV-labeled inputs to A1 L6 CT neurons were immunolabeled for ChAT and NeuN. Left panel: BLA = basolateral amygdala. Int = internal capsule. Scale bar, 0.5 mm. Right panels: higher magnification zoom of the area identified with the dashed square at left. Green arrows denote RV+ cells that do not express ChAT. Dual color arrows denote RV+/ChAT+ cells. Scale bar, 0.1 mm.
(B) The fraction of RV+ input cells that also expressed ChAT were calculated for five brain areas.

began hundreds of milliseconds prior to movement onset, not during movement (Figures 3B–3E, 4C, and 4D). Definitive proof of the anatomical inputs that route motor preparatory inputs into L6 CT neurons awaits gain- and loss-of-function experiments that directly activate and inactivate candidate brain areas. Here, we found that the strongest candidate for motor-related inputs came from the external globus pallidus, which featured approximately ten times more RV-labeled input neurons than M2. The relative paucity of direct input from M2 compared with what might be expected from previous work[14,40] could reflect different sources of motor-related inputs onto L6 CT versus other cortical cell types, or the tropism of our virus that resulted in poor transduction of M2 input neurons, or that prior characterizations were focused on different cortical fields within the mouse ACtx.

Another caveat in interpreting the findings reported here is that it is not entirely clear what conditions are necessary to elicit strong L6 activity prior to self-initiated movements. Self-initiated running bouts did not elicit strong L6 CT ensemble responses (Figures 4E and 4F), so one critical factor could be orofacial movements versus whole-body movements. On the other hand, the internal state of the mouse was not matched between these behaviors. By randomly assigning sounds and rewards to licks, the lick spout sampling task was an efficient design to elicit many trials per session that could be analyzed separately with respect to movement, sound stimulation, and reward. However, the task design also created an internal state where water-deprived mice were aware that water rewards were likely to occur, yet were highly uncertain from trial to trial whether contact with the lick spout would produce a sound and/or reward. The combination of increased motivation, uncertainty, and the arbitrary pairing of an unnatural sound (FM sweep) to movement at an arbitrary time delay could also be a key factor in eliciting strong motor-preparatory responses from L6 CT units. This fits with previous work showing that brainstem circuits cancel out reafferent sensory input when the acoustic consequences of movement are nearly immediate and highly stereotyped,[55] but that cortical circuits may be recruited when sensorimotor contingencies are flexible, arbitrary, unpredictable, and acquired through learning.[30,56] Future work could distill the critical ingredient(s) for extra-sensory activation of L6 CT neurons by recording during a much wider array of natural movements and explicitly varying the timing, predictability, and meaning of movement-triggered sounds.

STAR★METHODS

Detailed methods are provided in the online version of this paper and include the following:

- KEY RESOURCES TABLE
- RESOURCE AVAILABILITY
  - Lead Contact
  - Materials Availability
  - Data and Code Availability
- EXPERIMENTAL MODEL AND SUBJECT DETAILS
- METHOD DETAILS
  - Recovery surgeries
  - Lick spout sampling task
  - Treadmill running
  - Two-photon calcium imaging
  - Two-photon imaging analysis
  - Virus mediated gene-delivery
  - Preparation for single unit-recordings in head-fixed mice
  - Single unit recordings in head-fixed mice
  - Single unit recording analysis
  - Capture and quantification of orofacial movements
  - Anatomy
- QUANTIFICATION AND STATISTICAL ANALYSIS

SUPPLEMENTAL INFORMATION

Supplemental Information can be found online at https://doi.org/10.1016/j.cub.2020.10.027.

ACKNOWLEDGMENTS

We thank Evan Foss and Ishmael Stefanov for contributing to behavioral hardware development and Eyal Kimchi for guidance on using DeepLabCut. We thank D. Schneider for comments on an earlier version of the manuscript. We thank D. Kim and the Genetically Encoded Neuronal Indicator and Effector Project at the HHMI's Janelia Farm Research Campus for making the Thy1-GCaMP6s mouse publicly available. AAV5-Ef1a-DIO hChR2(E123T/T159C)-EYFP was developed by Karl Deisseroth. This work was supported by The Nancy Lurie Marks Family Foundation (D.B.P.); NIH grants DC017178 (D.B.P.), DC015388 (T.A.H.), and DC018327 (R.S.W.); NSF fellowship DGE1745303 (K.K.C.); and NIH fellowship DC015376 (R.S.W.).

AUTHOR CONTRIBUTIONS

K.C.C. and R.S.W. performed all experiments and analyses on live animals with supervisory input from D.B.P. T.A.H. performed imaging and analysis of fixed tissue. G.T. and A.M. contributed the viral tracing reagents and technical oversight on their appropriate use. K.E.H. developed neurobehavioral software control. D.B.P. and K.K.C. wrote the manuscript with feedback from all authors.

DECLARATION OF INTERESTS

The authors declare no competing interests.

Received: August 27, 2020
Revised: October 6, 2020
Accepted: October 8, 2020
Published: November 5, 2020

REFERENCES

1. Ramon y Cajal, S. (1906). The structure and connexions of neurons. https://www.nobelprize.org/prizes/medicine/1906/cajal/lecture/.
2. Olsen, S.R., Bortone, D.S., Adesnik, H., and Scanziani, M. (2012). Gain control by layer six in cortical circuits of vision. Nature *483*, 47–52.
3. Crandall, S.R., Cruikshank, S.J., and Connors, B.W. (2015). A corticothalamic switch: controlling the thalamus with dynamic synapses. Neuron *86*, 768–782.
4. Guo, W., Clause, A.R., Barth-Maron, A., and Polley, D.B. (2017). A corticothalamic circuit for dynamic switching between feature detection and discrimination. Neuron *95*, 180–194.e5.
5. Voigts, J., Deister, C.A., and Moore, C.I. (2019). Layer 6 ensembles can selectively regulate the behavioral impact and layer-specific representation of sensory deviants. bioRxiv. https://doi.org/10.1101/657114.
6. Vélez-Fort, M., Rousseau, C.V., Niedworok, C.J., Wickersham, I.R., Rancz, E.A., Brown, A.P.Y., Strom, M., and Margrie, T.W. (2014). The stimulus selectivity and connectivity of layer six principal cells reveals cortical microcircuits underlying visual processing. Neuron *83*, 1431–1443.
7. Gong, S., Doughty, M., Harbaugh, C.R., Cummins, A., Hatten, M.E., Heintz, N., and Gerfen, C.R. (2007). Targeting Cre recombinase to specific neuron populations with bacterial artificial chromosome constructs. J. Neurosci. *27*, 9817–9823.
8. Kim, J., Matney, C.J., Blankenship, A., Hestrin, S., and Brown, S.P. (2014). Layer 6 corticothalamic neurons activate a cortical output layer, layer 5a. J. Neurosci. *34*, 9656–9664.
9. Bortone, D.S., Olsen, S.R., and Scanziani, M. (2014). Translaminar inhibitory cells recruited by layer 6 corticothalamic neurons suppress visual cortex. Neuron *82*, 474–485.
10. Denman, D.J., and Contreras, D. (2015). Complex effects on in vivo visual responses by specific projections from mouse cortical layer 6 to dorsal lateral geniculate nucleus. J. Neurosci. *35*, 9265–9280.
11. Kirchgessner, M.A., Franklin, A.D., and Callaway, E.M. (2020). Context-dependent and dynamic functional influence of corticothalamic pathways to first- and higher-order visual thalamus. Proc Natl Acad Sci *117*, 13066–13077.
12. Williamson, R.S., and Polley, D.B. (2019). Parallel pathways for sound processing and functional connectivity among layer 5 and 6 auditory corticofugal neurons. eLife *8*, e42974.
13. Pauzin, F.P., and Krieger, P. (2018). A corticothalamic circuit for refining tactile encoding. Cell Rep. *23*, 1314–1325.
14. Schneider, D.M., Nelson, A., and Mooney, R. (2014). A synaptic and circuit basis for corollary discharge in the auditory cortex. Nature *513*, 189–194.
15. Llano, D.A., and Sherman, S.M. (2008). Evidence for nonreciprocal organization of the mouse auditory thalamocortical-corticothalamic projection systems. J. Comp. Neurol. *507*, 1209–1227.
16. Cai, D., Yue, Y., Su, X., Liu, M., Wang, Y., You, L., Xie, F., Deng, F., Chen, F., Luo, M., and Yuan, K. (2019). Distinct Anatomical Connectivity Patterns Differentiate Subdivisions of the Nonlemniscal Auditory Thalamus in Mice. Cereb. Cortex *29*, 2437–2454.
17. Prieto, J.J., and Winer, J.A. (1999). Layer VI in cat primary auditory cortex: Golgi study and sublaminar origins of projection neurons. J. Comp. Neurol. *404*, 332–358.
18. Winer, J.A., Diehl, J.J., and Larue, D.T. (2001). Projections of auditory cortex to the medial geniculate body of the cat. J. Comp. Neurol. *430*, 27–55.
19. Lima, S.Q., Hromádka, T., Znamenskiy, P., and Zador, A.M. (2009). PINP: a new method of tagging neuronal populations for identification during in vivo electrophysiological recording. PLoS ONE *4*, e6099.
20. Li, N., Chen, T.-W., Guo, Z.V., Gerfen, C.R., and Svoboda, K. (2015). A motor cortex circuit for motor planning and movement. Nature *519*, 51–56.
21. Guo, W., Robert, B., and Polley, D.B. (2019). The cholinergic basal forebrain links auditory stimuli with delayed reinforcement to support learning. Neuron *103*, 1164–1177.e6.
22. Augustinaite, S., and Kuhn, B. (2020). Complementary Ca2+ Activity of Sensory Activated and Suppressed Layer 6 Corticothalamic Neurons Reflects Behavioral State. Curr. Biol. *30*, 1–16.
23. Pauzin, F.P., Schwarz, N., and Krieger, P. (2019). Activation of corticothalamic layer 6 cells decreases angular tuning in mouse barrel cortex. Front. Neural Circuits *13*, 67.
24. Sundberg, S.C., Lindström, S.H., Sanchez, G.M., and Granseth, B. (2018). Cre-expressing neurons in visual cortex of Ntsr1-Cre GN220 mice are corticothalamic and are depolarized by acetylcholine. J. Comp. Neurol. *526*, 120–132.
25. Tasic, B., Yao, Z., Graybuck, L.T., Smith, K.A., Nguyen, T.N., Bertagnolli, D., Goldy, J., Garren, E., Economo, M.N., Viswanathan, S., et al. (2018). Shared and distinct transcriptomic cell types across neocortical areas. Nature *563*, 72–78.
26. French, C.A., and Fisher, S.E. (2014). What can mice tell us about Foxp2 function? Curr. Opin. Neurobiol. *28*, 72–79.
27. Zhou, M., Liang, F., Xiong, X.R., Li, L., Li, H., Xiao, Z., Tao, H.W., and Zhang, L.I. (2014). Scaling down of balanced excitation and inhibition by active behavioral states in auditory cortex. Nat. Neurosci. *17*, 841–850.
28. McGinley, M.J., David, S.V., and McCormick, D.A. (2015). Cortical membrane potential signature of optimal states for sensory signal detection. Neuron *87*, 179–192.
29. Rummell, B.P., Klee, J.L., and Sigurdsson, T. (2016). Attenuation of responses to self-generated sounds in auditory cortical neurons. J. Neurosci. *36*, 12010–12026.
30. Schneider, D.M., Sundararajan, J., and Mooney, R. (2018). A cortical filter that learns to suppress the acoustic consequences of movement. Nature *561*, 391–395.

31. Bigelow, J., Morrill, R.J., Dekloe, J., and Hasenstaub, A.R. (2019). Movement and VIP interneuron activation differentially modulate encoding in mouse auditory cortex. eNeuro *6*, https://doi.org/10.1523/ENEURO.0164-19.2019.

32. Mathis, A., Mamidanna, P., Cury, K.M., Abe, T., Murthy, V.N., Mathis, M.W., and Bethge, M. (2018). DeepLabCut: markerless pose estimation of user-defined body parts with deep learning. Nat. Neurosci. *21*, 1281–1289.

33. Nath, T., Mathis, A., Chen, A.C., Patel, A., Bethge, M., and Mathis, M.W. (2019). Using DeepLabCut for 3D markerless pose estimation across species and behaviors. Nat. Protoc. *14*, 2152–2176.

34. Daigle, T.L., Madisen, L., Hage, T.A., Valley, M.T., Knoblich, U., Larsen, R.S., Takeno, M.M., Huang, L., Gu, H., Larsen, R., et al. (2018). A suite of transgenic driver and reporter mouse lines with enhanced brain-cell-type targeting and functionality. Cell *174*, 465–480.e22.

35. Liang, Y., Sun, W., Lu, R., Chen, M., and Ji, N. (2019). A distinct population of L6 neurons in mouse V1 mediate cross-callosal communication. bioRxiv. https://doi.org/10.1101/778019.

36. Yang, Y., Lee, J., and Kim, G. (2020). Integration of locomotion and auditory signals in the mouse inferior colliculus. eLife *9*, 1–17.

37. Nelson, A., and Mooney, R. (2016). The Basal Forebrain and Motor Cortex Provide Convergent yet Distinct Movement-Related Inputs to the Auditory Cortex. Neuron *90*, 635–648.

38. Kuchibhotla, K.V., Gill, J.V., Lindsay, G.W., Papadoyannis, E.S., Field, R.E., Sten, T.A.H., Miller, K.D., and Froemke, R.C. (2017). Parallel processing by cortical inhibition enables context-dependent behavior. Nat. Neurosci. *20*, 62–71.

39. Abs, E., Poorthuis, R.B., Apelblat, D., Muhammad, K., Pardi, M.B., Enke, L., Kushinsky, D., Pu, D.L., Eizinger, M.F., Conzelmann, K.K., et al. (2018). Learning-related plasticity in dendrite-targeting layer 1 interneurons. Neuron *100*, 684–699.e6.

40. Nelson, A., Schneider, D.M., Takatoh, J., Sakurai, K., Wang, F., and Mooney, R. (2013). A circuit for motor cortical modulation of auditory cortical activity. J. Neurosci. *33*, 14342–14353.

41. Lee, I.H., and Assad, J.A. (2003). Putaminal activity for simple reactions or self-timed movements. J. Neurophysiol. *89*, 2528–2537.

42. Dodson, P.D., Larvin, J.T., Duffell, J.M., Garas, F.N., Doig, N.M., Kessaris, N., Duguid, I.C., Bogacz, R., Butt, S.J.B., and Magill, P.J. (2015). Distinct developmental origins manifest in the specialized encoding of movement by adult neurons of the external globus pallidus. Neuron *86*, 501–513.

43. Saunders, A., Oldenburg, I.A., Berezovskii, V.K., Johnson, C.A., Kingery, N.D., Elliott, H.L., Xie, T., Gerfen, C.R., and Sabatini, B.L. (2015). A direct GABAergic output from the basal ganglia to frontal cortex. Nature *521*, 85–89.

44. Abecassis, Z.A., Berceau, B.L., Win, P.H., García, D., Xenias, H.S., Cui, Q., Pamukcu, A., Cherian, S., Hernández, V.M., Chon, U., et al. (2020). Npas1+-Nkx2.1+ neurons are an integral part of the cortico-pallido-cortical loop. J. Neurosci. *40*, 743–768.

45. Chavez, C., and Zaborszky, L. (2017). Basal forebrain cholinergic-auditory cortical network: primary versus nonprimary auditory cortical areas. Cereb. Cortex *27*, 2335–2347.

46. Wickersham, I.R., Lyon, D.C., Barnard, R.J.O., Mori, T., Finke, S., Conzelmann, K.K., Young, J.A.T., and Callaway, E.M. (2007). Monosynaptic restriction of transsynaptic tracing from single, genetically targeted neurons. Neuron *53*, 639–647.

47. Wall, N.R., Wickersham, I.R., Cetin, A., De La Parra, M., and Callaway, E.M. (2010). Monosynaptic circuit tracing in vivo through Cre-dependent targeting and complementation of modified rabies virus. Proc. Natl. Acad. Sci. USA *107*, 21848–21853.

48. Tasaka, G.I., Feigin, L., Maor, I., Groysman, M., DeNardo, L.A., Schiavo, J.K., Froemke, R.C., Luo, L., and Mizrahi, A. (2020). The temporal association cortex plays a key role in auditory-driven maternal plasticity. Neuron *107*, 566–579.e7.

49. Miyamichi, K., Shlomai-Fuchs, Y., Shu, M., Weissbourd, B.C., Luo, L., and Mizrahi, A. (2013). Dissecting local circuits: parvalbumin interneurons underlie broad feedback control of olfactory bulb output. Neuron *80*, 1232–1245.

50. Kim, E.J., Jacobs, M.W., Ito-Cole, T., and Callaway, E.M. (2016). Improved monosynaptic neural circuit tracing using engineered rabies virus glycoproteins. Cell Rep. *15*, 692–699.

51. Andersen, R.A., Knight, P.L., and Merzenich, M.M. (1980). The thalamocortical and corticothalamic connections of AI, AII, and the anterior auditory field (AAF) in the cat: evidence for two largely segregated systems of connections. J. Comp. Neurol. *194*, 663–701.

52. Morrill, R.J., and Hasenstaub, A.R. (2018). Visual information present in infragranular layers of mouse auditory cortex. J. Neurosci. *38*, 2854–2862.

53. Hangya, B., Ranade, S.P., Lorenc, M., and Kepecs, A. (2015). Central cholinergic neurons are rapidly recruited by reinforcement feedback. Cell *162*, 1155–1168.

54. Mease, R.A., Krieger, P., and Groh, A. (2014). Cortical control of adaptation and sensory relay mode in the thalamus. Proc. Natl. Acad. Sci. USA *111*, 6798–6803.

55. Singla, S., Dempsey, C., Warren, R., Enikolopov, A.G., and Sawtell, N.B. (2017). A cerebellum-like circuit in the auditory system cancels responses to self-generated sounds. Nat. Neurosci. *20*, 943–950.

56. Schneider, D.M., and Mooney, R. (2018). How movement modulates hearing. Annu. Rev. Neurosci. *41*, 553–572.

57. Romero, S., Hight, A.E., Clayton, K.K., Resnik, J., Williamson, R.S., Hancock, K.E., and Polley, D.B. (2020). Cellular and Widefield Imaging of Sound Frequency Organization in Primary and Higher Order Fields of the Mouse Auditory Cortex. Cereb. Cortex *30*, 1603–1622.

58. Pachitariu, M., Steinmetz, N., Kadir, S., Carandini, M., and Harris, K.D. (2016). Kilosort: realtime spike-sorting for extracellular electrophysiology with hundreds of channels. bioRxiv. https://doi.org/10.1101/061481.

59. Friedrich, J., Zhou, P., and Paninski, L. (2017). Fast online deconvolution of calcium imaging data. PLoS Comput. Biol. *13*, e1005423.

60. Williamson, R.S., Hancock, K.E., Shinn-Cunningham, B.G., and Polley, D.B. (2015). Locomotion and task demands differentially modulate thalamic audiovisual processing during active search. Curr. Biol. *25*, 1885–1891.

61. Hackett, T.A., Barkat, T.R., O'Brien, B.M.J., Hensch, T.K., and Polley, D.B. (2011). Linking topography to tonotopy in the mouse auditory thalamocortical circuit. J. Neurosci. *31*, 2983–2995.

62. Müller-Preuss, P., and Mitzdorf, U. (1984). Functional anatomy of the inferior colliculus and the auditory cortex: current source density analyses of click-evoked potentials. Hear. Res. *16*, 133–142.

63. Metherate, R., Kaur, S., Kawai, H., Lazar, R., Liang, K., and Rose, H.J. (2005). Spectral integration in auditory cortex: mechanisms and modulation. Hear. Res. *206*, 146–158.

64. Schmitzer-Torbert, N., Jackson, J., Henze, D., Harris, K., and Redish, A.D. (2005). Quantitative measures of cluster quality for use in extracellular recordings. Neuroscience *131*, 1–11.

65. Lein, E.S., Hawrylycz, M.J., Ao, N., Ayres, M., Bensinger, A., Bernard, A., Boe, A.F., Boguski, M.S., Brockway, K.S., Byrnes, E.J., et al. (2007). Genome-wide atlas of gene expression in the adult mouse brain. Nature *445*, 168–176.

Please cite this article in press as: Clayton et al., Auditory Corticothalamic Neurons Are Recruited by Motor Preparatory Inputs, Current Biology (2020), https://doi.org/10.1016/j.cub.2020.10.027

STAR★METHODS

KEY RESOURCES TABLE

REAGENT or RESOURCE	SOURCE	IDENTIFIER
Antibodies		
Mouse anti-NeuN	Millipore	MAB377; RRID: AB_2298772
Goat anti-ChAT	Millipore	AB144P; RRID: AB_2079751
Goat anti FoxP2	Novus	55411; RRID: AB_2107125
Donkey anti-mouse, Alexa 647	Lifetech	A329; RRID: AB_162542
Donkey anti-goat, Alexa 647	Lifetech	A32789; RRID: AB_2535864
Bacterial and Virus Strains		
AAV5-Ef1a-DIO hChR2(E123T/T159C)-EYFP	Addgene	35509-AAV5
AAV2-CAG-Flex-TVA	Adi Mizrahi	N/A
AAV2-CAG-Flex-oPGB	Adi Mizrahi	N/A
Sad-delta-G	Adi Mizrahi	N/A
Chemicals, Peptides, and Recombinant Proteins		
Lidocaine hydrochloride	Hospira Inc	Cat# 71-157-DK
Buprenorphine hydrochloride	Buprenex	Cat#NDC 12496-0757-5
Isoflurane	Piramal	Cat#NDC 66794-013-10
Flow-It ALC Flowable Composite	Pentron	Cat#N11B
C&B Metabond Quick Adhesive Cement System	Parkell	Cat#S380
Silicon adhesive	WPI	Cat#KWIK-SIL
Prolong Gold antifade media	Lifetech	Cat# P36930
Experimental Models: Organisms/Strains		
Mouse:Ntsr1-Cre	GENSAT	B6.FVB(Cg)-Tg(Ntsr1-Cre)GN220Gsat/Mcd
Mouse: Ai148D: B66.Cg-Igs7tm148.1(tetO-GCaMP6f, CAG-tTA2)Hze/J	The Jackson Laboratory	RRID:IMSR_JAX:030328
Mouse: Tg(Thy1-GCaMP6s)GP4.3Dkim	The Jackson Laboratory	RRID:IMSR_JAX:024275
Mouse: CBA/CaJ	The Jackson Laboratory	RRID:IMSR_JAX:000654)
Deposited Data		
Preprocessed dataset	N/A	https://doi.org/10.17632/d6xvxypx95.1
Software and Algorithms		
Labview 2015	National Instruments	https://www.ni.com/en-us/shop/labview.html
Synapse	Tucker-Davis Technologies	http://www.tdt.com/component/synapse-software/
ThorImage 3.0	Thorlabs	https://www.thorlabs.com/newgrouppage9.cfm?objectgroup_id=9072#ad-image-0
Kilosort	Github	https://github.com/cortex-lab/Kilosort
Suite2P	Github	https://github.com/cortex-lab/Suite2P
DeepLabCut	Github	https://github.com/DeepLabCut/DeepLabCut
MATLAB 2016b	Mathworks	https://www.mathworks.com/products/matlab.html
Python 3.7	Python	https://www.python.org/downloads/release/python-370/
Other		
Linear silicone recording electrode	Cambridge Neurotech	H3
Linear silicone recording electrode	NeuroNexus	NeuroNexus A1x16-50-177-5mm
Diode laser (473 nm)	Omnicon	LuxX_473-100
PZ5 Neurodigitizer amplifier	Tucker-Davis Technologies	Pz-128
BioAmp processor	Tucker-Davis Technologies	RZ5D
Power meter	Thorlabs	S120C
Solenoid driver	Eaton-Peabody Lab	https://github.com/EPL-Engineering/epl_valve

(*Continued on next page*)

Please cite this article in press as: Clayton et al., Auditory Corticothalamic Neurons Are Recruited by Motor Preparatory Inputs, Current Biology (2020), https://doi.org/10.1016/j.cub.2020.10.027

Continued

REAGENT or RESOURCE	SOURCE	IDENTIFIER
Lickometer	Eaton-Peabody Lab	https://github.com/EPL-Engineering/epl_lickometer
PXI Controller	National Instruments	PXIe-8840
Free-field speaker	Parts Express	275-010
Ti-Sapphire laser	Spectra Physics	Mai Tai HP DeepSee
16x/.8NA Objective	Nikon	CFI75 LWD 16X W
Two-Photon Microscope	Thorlabs	Bergamo
Titanium headplate	iMaterialise	Custom
IR Camera	Sony	Playstation Eye
LED driver	Thorlabs	Cat# LEDD1B

RESOURCE AVAILABILITY

Lead Contact

Further information and requests should be directed to and will be fulfilled by the lead contact, Daniel Polley (daniel_polley@meei.harvard.edu).

Materials Availability

This study did not generate new reagents.

Data and Code Availability

Data acquisition and analysis was performed with custom scripts in MATLAB, LabVIEW, and Python. Spike sorting was done in Kilosort (https://github.com/cortex-lab/Kilosort). Two photon imaging ROI extraction and spike deconvolution was done in Suite2p (https://github.com/cortex-lab/Suite2P). Markerless behavior tracking was done with DeepLabCut (https://github.com/DeepLabCut/DeepLabCut). Original data have been deposited to Mendeley Data: https://doi.org/10.17632/d6xvxypx95.1.

EXPERIMENTAL MODEL AND SUBJECT DETAILS

All procedures were approved by the Massachusetts Eye and Ear Animal Care and Use Committee and followed the guidelines established by the National Institutes of Health for the care and use of laboratory animals. Mice of both sexes were used for this study. All mice were maintained on a 12 h light/12 h dark cycle with *ad libitum* access to food and water, unless undergoing behavioral testing. Mice undergoing behavioral testing were kept on a reversed 12 h light (7:00 a.m.-7:00 p.m) /12 h dark cycle. Mice were grouped housed unless they had undergone a major survival surgery.

For 2-photon imaging experiments, we used 5 Thy1-GCaMP6sxCBA-CaJ mice and 6 NTSR1-Cre x Ai148 mice. For single-unit electrophysiology experiments, we used 7 NTSR1-Cre mice. For anatomy experiments, we used 3 NTSR1-Cre x Ai148 mice (FoxP2 labeling) and 5 NTRS1-Cre mice (RV tracing).

METHOD DETAILS

Recovery surgeries

Mice were anesthetized with isoflurane in oxygen (5% induction, 2% maintenance). A homeothermic blanket system maintained body temperature at 36.5° (FHC). Lidocaine hydrochloride was administered subcutaneously to numb the scalp. The dorsal surface of the scalp was retracted and the periosteum was removed. For mice to be used in behavior and physiology experiments, the skull surface was prepped with etchant (C&B metabond) and 70% ethanol before affixing a titanium head plate (iMaterialise) to the dorsal surface with dental cement (C&B metabond). At the conclusion of all recovery procedures, Buprenex (.05 mg/kg) and meloxicam (0.1 mg/kg) were administered and the animal was transferred to a warmed recovery chamber.

Lick spout sampling task

Three days after headplate surgery, animals were weighed and placed on a water restriction schedule (1 mL per day). During behavioral training, animals were weighed daily to ensure they remained above 80% of their initial weight and examined for signs of dehydration. Mice were given supplemental water if they received less than 1 mL during a training session. Mice were head-fixed in a dimly lit, single-walled sound-attenuating booth (Acoustic Systems), with their bodies resting in conductive cradle. The lick spout apparatus consisted of a single spout positioned 1 cm below the animal's snout using a 3D micromanipulator (Thorlabs). Tongue contact on the lick spout closed an electrical circuit that was digitized at 400 Hz and encoded to calculate lick timing. For electrophysiology experiments, an infrared photobeam emitter/detector for was used to avoid electrical artifacts. Acoustic stimuli were delivered through inverted

Please cite this article in press as: Clayton et al., Auditory Corticothalamic Neurons Are Recruited by Motor Preparatory Inputs, Current Biology (2020), https://doi.org/10.1016/j.cub.2020.10.027

dome tweeters positioned 10 cm from the animal's left ear (CUI, CMS0201KLX). Digital and analog signals controlling sound delivery and water reward were controlled by a PXI system with custom software programed in LabVIEW (National Instruments). Free-field stimuli were calibrated before recording using a wide-band ultrasonic acoustic sensor (Knowles Acoustics, model SPM0204UD5).

Mice were initially conditioned to lick the spout to receive a 4-6 μL bolus of water 0.5 s later. Once mice reliably licked to receive reward, we varied the outcome such that 50% of lick bouts triggered a sound and 50% of lick bouts resulted in reward. Because trials with water reward are associated with longer lick duration and additional reinforcement-related activity, we only analyzed trials without water reward. Sound and reward probability were determined independently. Sound onset was delayed by 0.1 s following lick bout initiation. Rapid frequency modulated sweeps were used in these experiments because they elicited strong A1 neural responses across a wide range of best frequency tuning (50 ms sweeps presented at 70 dB SPL; 4:64 kHz range [80 octaves/s], 5ms raised cosine onset/offset ramps). To avoid photobleaching, 2-photon imaging sessions were limited to 135 trials per day (approximately 30 min) by only presenting upward FM sweeps. For electrophysiology and video tracking experiments, 200-500 trials were performed each day and included both upward and downward FM sweeps. Continuous broadband noise (50 dB SPL) was used to mask sounds generated by licking.

Treadmill running

Head-fixed mice were habituated to running on a low-inertia, quiet cylindrical treadmill over 4-6d period before neural recordings began. Locomotion was recorded using an optical rotary encoder. Locomotion signals were downsampled to 30 Hz and filtered using a zero-phase digital filter. Locomotion was operationally defined as periods where running speed exceeded 2 cm/s. Exceeding the locomotion threshold had a 50% chance of triggering an upward FM sweep (stimulus characteristics as described above). Locomotion-related activity was only analyzed on trials without sound delivery. Water was not delivered during locomotion. In order for trials to be included for analysis, at least 3 s of quiescence were required prior a running bout that lasted for a minimum of 1 s. Only sessions that included at least 15 locomotion bouts were used in the analysis. Continuous broadband noise (50 dB SPL) was used to mask sounds generated by running.

Two-photon calcium imaging

Three round glass coverslips (one 4mm, two 3mm, #1 thickness, Warner Instruments) were etched with piranha solution and bonded into a vertical stack using transparent, UV-cured adhesive (Norland Products, Warner Instruments). Headplate attachment, anesthesia and analgesia follow the procedure listed above. A 3 mm craniotomy was made over right ACtx using a scalpel and the coverslip stack was cemented into the craniotomy (C&B Metabond). Animals recovered for at least 5 days before beginning water restriction for the lick spout sampling task.

An initial widefield epifluorescence imaging session was performed to visualize the tonotopic gradients of the ACtx and identify the position of A1 as described previously.[57] Two-photon excitation was provided by a Mai-Tai eHP DS Ti:Sapphire-pulsed laser tuned to 940 nm (Spectra-Physics). Imaging was performed with a 16 × /0.8NA water-immersion objective (Nikon) from a 512 × 512 pixel field of view at 30Hz with a Bergamo II Galvo-Resonant 8 kHz scanning microscope (Thorlabs). Scanning software (Thorlabs) was synchronized to the stimulus generation hardware (National Instruments) with digital pulse trains. Widefield and 2-photon microscopes were rotated by 50-60 degrees off the vertical axis to obtain images from the lateral aspect of the mouse cortex while the animal was maintained in an upright head position. Imaging was performed in light-tight, sound attenuating chambers. Animals were monitored throughout the experiment to confirm all imaging was performed in the awake condition using modified cameras (PlayStation Eye, Sony) coupled to infrared light sources.

For 2-photon imaging of L2/3 PyrNs, imaging was performed 175-225 μm below the pial surface. The focal plane for L6 imaging was 600-700 μm below the pial surface, which can be accomplished with relatively low excitation power (107-138 mW) because Ntsr1-Cre neurons have sparse apical dendritic fields that produce minimal out of plane excitation.[5,22,34,35] The DeepSee precompensation oscillator (Spectra Physics) was adjusted for each imaging session to improve image quality and reduce laser power for L6 imaging.

Fluorescence images were captured at 2 × digital zoom. Raw calcium movies were processed using Suite2P, a publicly available analysis pipeline.[58] Briefly, movies are registered to account for brain motion. Regions of interest are established by clustering neighboring pixels with similar time courses. Manual curation is then performed in the Suite2P GUI to eliminate low quality or non-somatic ROIs. Spike deconvolution was performed in Suite2P, using the default method based on the OASIS algorithm.[59]

Two-photon imaging analysis

Sound-responsive neurons were identified by measuring deconvolved activity during a pre-stimulus (−133 - 0ms prior to sound onset) and post-stimulus period (33 - 167ms following sound onset) in sound alone trials. Sound responsive neurons were operationally defined as having significantly elevated activity in the post-stimulus period based on a one-tailed paired-test ($p < 0.05$). To calculate sound-evoked activity rates for sound alone and sound + lick conditions, the baseline activity level during the pre-stimulus window was subtracted from the post-stimulus window.

The modulation index for sound-evoked activity was calculated as:

$$Modulationindex = \frac{Soundalone - Soundandlick}{Soundalone + SoundandLick}$$

To calculate activity rates during lick only conditions, we first defined baseline activity during a 0.5 s period that was separated by at least 2 s from the last lick of a preceding bout and 1.5 s from the first lick of an upcoming bout. Lick-related activity was calculated

Please cite this article in press as: Clayton et al., Auditory Corticothalamic Neurons Are Recruited by Motor Preparatory Inputs, Current Biology (2020), https://doi.org/10.1016/j.cub.2020.10.027

during a 1.5 s period beginning 1 s prior to lick onset, where mean activity in each 33ms time bin was expressed in units of z-score relative to the baseline distribution. Neurons were classified as significantly enhanced or suppressed during licking by calculating the mean activity rates during a period of licking (−0.5 to 0.5 s relative to lick onset) versus a period of quiescence (−2 to −1 s relative to lick onset) based on a $p < 0.05$ threshold of a two-tailed Wilcoxon rank-sum test.

Virus mediated gene-delivery

For mice used in optogenetics experiments, two burr holes (< 1mm diameter each) were made in the skull overlying A1 in the right hemisphere, 1.75 - 2.25mm rostral to the lambdoid suture. A motorized injection system (Stoelting) was used to inject 200nL of AAV5-Ef1a-DIO hChR2(E123T/T159C)-EYFP into each burr hole 600 μm below the pial surface. Electrophysiology experiments began 3-4 weeks after injection. For anatomical tracing experiments using pseudotyped rabies virus, 150 nL of a 1:2 mixture AAV2-CAG-FLEx-TVA-mCherry and AAV2-CAG-FLEx-oG were injected through a single burr hole, 600 μm below the surface of A1. After a 14-21 day waiting period, we targeted the same location and depth for a second injection of SAD-ΔG-GFP (500nL). Mice were perfused 4 days after the SAD-ΔG injection. Immediately following each injection, the scalp was sutured and the animal recovered in a warmed chamber. All virus solutions were injected at a rate of 15nL/min.

Preparation for single unit-recordings in head-fixed mice

A ground wire (AgCl) was implanted over the left occipital cortex. A craniotomy was made above the right MGB (centered 2.75 mm lateral to the midline and 2.75 mm caudal to bregma) and the position of the ventral subdivision was identified with a cursory mapping of multiunit pure tone receptive fields as described previously.[4,12,60] An optic fiber (flat tip, 0.2mm diameter, Thorlabs) was inserted 2.4 – 2.8mm to rest 0.2mm above the physiologically identified dorsal surface of MGB. The fiber assembly was cemented in place and painted with black nail polish to prevent light leakage. Animals were allowed to recover for at least three days before water restriction began.

On the day of the first recording session, mice were briefly anaesthetized with isoflurane (2%) and a small craniotomy (0.5 medial-lateral x 1.25 mm rostral-caudal) was made over A1 in the right hemisphere, centered 2mm from the lambdoid suture. Each day, a small well was made around the craniotomy with UV-cured cement and filled with lubricating ointment (Paralub Vet Ointment). At the conclusion of each recording, the chamber was flushed, filled with new ointment, and capped with UV-cured cement.

Single unit recordings in head-fixed mice

A 64-channel silicon probe (H3, Cambridge Neurotech) was slowly advanced (100 μm/s) into ACtx perpendicular to the pial surface until the tip of the electrode was 1.3-1.4mm below the cortical surface, ensuring full coverage of all layers of A1. The brain was allowed to settle for at least 15 min before recordings began. On the day of the first recording, multiple penetrations were made to identify the tonotopic reversal which represents the rostral border of A1.[61]

Raw neural data was digitized at 32-bit, 24.4 kHz and stored in binary format (PZ5 Neurodigitizer, RZ2 BioAmp Processor, RS4 Data Streamer; Tucker-Davis Technologies). To eliminate artifacts, the common mode signal (channel-averaged neural traces) was subtracted from all channels in the brain. Signals were notch filtered at 60Hz, then band-pass filtered (300-3000 Hz, second order Butterworth filters). To calculate local field potentials, raw signals were first notch filtered at 60 Hz and downsampled to 1 kHz. The CSD was calculated as the second spatial derivative of the LFP signal. To eliminate potential artifacts introduced by impedance mismatching between channels, signals were spatially smoothed along the channels with a triangle filter (5-point Hanning window). Two CSD signatures were used to identify L4 in accordance with prior studies: A brief current sink first occurs approximately 10ms after the onset of broadband noise burst, which was used to determine the lower border of L4 (50ms duration, 70 dB SPL, 50 trials). A tri-phasic CSD pattern (sink-source-sink from upper to lower channels) occurs between 20ms and 50ms, where the border between the upper sink and the source was used to define the upper boundary of L4.[4,62,63]

Kilosort was used to sort spikes into single unit clusters.[58] Single-unit isolation was based on the presence of both a refractory period within the interspike interval histogram, and an isolation distance (> 10) indicating that single-unit clusters were well separated from the surrounding noise.[64] RS and FS designation was based on the ratio of the mean trough to peak interval > 0.6 (RS) or < 0.5 (FS). Ntsr1-Cre L6 corticothalamic units were identified using antidromic phototagging. A 1ms pulse of 473nm light was delivered via the implanted MGB fiber to fire antidromic spikes in L6 corticothalamic units that expressed hChR2 (5-45 mW laser power, repeated at 4Hz for 500 repetitions with a diode laser, Omicron, LuxX). Ntsr1-Cre+ L6 corticothalamic cells were distinguished from indirectly activated neurons based on laser-evoked spiking rates at least 5 SD above baseline and first spike latencies that varies by less than 0.35 SD, as confirmed in a previous study.[12]

Single unit recording analysis

Single unit spike times were binned at 200 Hz for sensory characterization and laser-evoked firing rate analyses. Sound- and laser-evoked spiking was referenced to the mean spike rate 100ms before stimulus onset. Frequency response areas for sound responsive units were obtained by presenting pseudorandomly ordered pure tones (50 ms duration, 4 ms raised cosine onset/offset ramps) of variable frequency (4–64 kHz in 0.5 octave increments) and level (0–60 dB SPL in 5 dB SPL increments). Each pure tone/level combination was repeated two times. Spikes were collected from the tone-driven portion of the PSTH and averaged across repetitions.

Single unit spike times for lick-related analyses were binned at 30 Hz for direct comparison with 2-photon and behavior tracking data. Units were excluded from further analysis if spontaneous spike rates were < 0.1 Hz. Sound-responsive units, evoked-activity

Please cite this article in press as: Clayton et al., Auditory Corticothalamic Neurons Are Recruited by Motor Preparatory Inputs, Current Biology (2020), https://doi.org/10.1016/j.cub.2020.10.027

rates and the modulation index for sound alone and sound + lick conditions were calculated similarly to the 2-photon data except that pre- and post-stimulus spike measurement windows were −66-0ms and 33-99ms relative to sound onset, respectively. Lick related activity was calculated with the same methods as described above for 2-photon imaging. Latencies of motor-related excitation or suppression was defined as the first time point that activity consistently exceeded the 5th or 95th percentile of the baseline spike rate distribution (as per Schneider et al., 2014[14]). Analyses was initiated at the minimum (suppressed) or maximum (enhanced) activity time bin and preceded backward in time until this condition was first met.

Capture and quantification of orofacial movements

Videos of the animal's face were obtained using a camera (Playstation Eye, Sony) coupled with infrared light sources (Thorlabs) and a 5-50 mm varifocal lens (Computar CS-Mount). Videos were acquired at 30 Hz (N = 2) or 60 Hz (N = 2) at a resolution of 512x512 pixels. A single point on the vibrissae array, nose, jaw, tongue and pinna were labeled alongside four cardinal positions on the circumference of the pupil in 60 frames for each imaging session. Manually labeled frames were split into training and test sets and the network was trained for 1.3 million iterations using default parameters in DeepLabCut.[32,33] Low-confidence outlier frames were manually re-labeled, the model re-trained and full video dataset reanalyzed. As the lower jaw and tongue markers were not visible until lick initiation, the point where they first appeared was manually entered as their position for all quiescent frames. Any remaining spurious position values where model confidence was < 0.9 was replaced with the interpolated value determined from surrounding frames.

Each tracked point was expressed as a 3-D vector as X × Y × Time. All videos recorded at 60Hz were downsampled to 30Hz for further analysis. Pupil diameter was calculated as the mean of the two diameter measurements. All other points were reduced to a 1-dimensional activity trace d(t) as:

$$d(t) = \sqrt{\left(\frac{x(t) - \bar{x}}{\sigma(x)}\right)^2 + \left(\frac{y(t) - \bar{y}}{\sigma(y)}\right)^2}$$

where x(t) is the x position at time point t and y(t) is the y position at time point t, which are normalized using the mean and the standard deviation of the entire x and y position traces respectively. A zero-phase digital filter was then used to smooth activity traces without introducing temporal distortions. Movement amplitude spectrum and coherence measurements were measured over the duration of each session. The tongue movement amplitude spectrum was obtained using the Fast-Fourier transform. The magnitude-squared coherence between tongue movements and other facial markers was computed using Welch's overlapped averaged periodogram method with a window size of 50 s and an overlap of 46.66 s. Movement onset latency was computed identically to motor-related neural latency, as described above.

Anatomy

Mice were deeply anaesthetized with ketamine and transcardially perfused using 4% paraformaldehyde in 0.01M phosphate buffered saline. Brains were extracted and post-fixed in 4% paraformaldehyde for 12 h, then placed in 30% sucrose. Brains were sectioned coronally at 40 μm into 0.1M phosphate buffer, preserving all sections containing cerebral cortex.

To co-localize Ntsr1-Cre and FoxP2 in NeuN-labled ACtx neurons, fluorescent immunohistochemistry assays were performed on sections of NTSR1 × Ai148 brains. Additional immunohistochemistry assays for cholineactyltransferse (ChAT) were performed on all sections of RV-injected brains. Sections were rinsed in 0.1M phosphate buffered saline (PBS), permeabilized for 2 h at room temperature in a blocking solution of 0.1M PBS, 2% BSA, 5% donkey serum, 0.1% Tween-20, then incubated for 48 h at 4°C in blocking solution containing the primary antibodies. Sections were rinsed in PBS then incubated for 2 h at room temperature in blocking solution containing secondary antibodies, counterstained in DAPI for 5 min, rinsed in 0.01M phosphate buffer, mounted onto glass slides, then coverslipped using Prolong Gold antifade media (Lifetech, Eugene OR).

ACtx sections were imaged in z stacks over 20 μm (2 μm steps) on a Nikon 90i epifluorescence microscope (40 × Plan Fluor, oil DIC N2). Co-localization of NeuN, Ntsr1-Cre labeled GFP, and FoxP2 were quantified in 0.25mm wide regions of L6 in A1. Labeled cells were counted independently for each fluorescence channel in two adjacent sections from each hemisphere of three brains using the Taxonomy function in Nikon Elements AR software. Analysis was restricted to NeuN-labled cells containing a DAPI-labeled nucleus.

To count and localize cells in RV-injected brains, all sections were scanned at 20 × using a Leica Versa widefield epifluorescence microscope, then converted to multichannel TIFF files for identification of labeled cells and brain areas. Reconstructions and cell counts were performed in layers using Adobe Illustrator, with reference to the Allen Brain Atlas[65] and the stereotaxic mouse brain atlases.

QUANTIFICATION AND STATISTICAL ANALYSIS

All statistical analyses were performed in MATLAB 2016b (Mathworks). Data are reported as mean ± SEM unless otherwise indicated. Non-parametric tests were used when data samples did not meet assumptions for parametric statistical tests. Inflated familywise error rates from multiple comparisons of the same sample were adjusted with the Holm-Bonferroni correction. Statistical significance was defined as $p < 0.05$.